Spring 2013

Growth and Carboxysome Composition of the Csosia Pore Mutants of *Halothiobacillus neapolitanus*

Jenifer Milam
University of Southern Mississippi

The University of Southern Mississippi

GROWTH AND CARBOXYSOME COMPOSITION OF THE CSOS1A PORE MUTANTS OF *HALOTHIOBACILLUS NEAPOLITANUS*

by

Jenifer Michelle Milam

A Thesis
Submitted to the Graduate School
of The University of Southern Mississippi
in Partial Fulfillment of the Requirements
for the Degree of Master of Science

Approved:

Dean of the Graduate School

May 2013

ABSTRACT

GROWTH AND CARBOXYSOME COMPOSITION OF THE CSOS1A PORE MUTANTS OF *HALOTHIOBACILLUS NEAPOLITANUS*

by Jenifer Michelle Milam

May 2013

Carboxysomes are specialized organelles that are filled with ribulose 1,5-bisphosphate carboxylase/oxygenase (RubisCO) needed for CO_2 fixation. The major carboxysome shell proteins, CsoS1A, B, and C, form hexamers which tile together to form the facets of the thin shell. Each hexamer has a small central pore that may play a role in metabolite flux. Using predicted structural models, a specific amino acid within the conserved hexamer pore motif (Phe-Val-Gly-Gly-Gly-Tyr) was chosen to change the size and charge of the pore, respectively. Two mutants of *Halothiobacillus neapolitanus* were generated in which the wild type *csoS1A* gene was replaced with the desired mutant allele. The first mutant, G42L, contained a Leu residue at position 42 (Phe-Val-Leu-Gly-Gly-Tyr) and was predicted to have a greatly reduced pore. Mutant F40D (Asp-Val-Gly-Gly-Gly-Tyr) was predicted to have CsoS1A hexamer pores of opposite surface charge. The growth of the pore mutant cultures determined if the altered hexamer pores affected carboxysome function in preparation for the future assessment of diffusion of RubisCO metabolites across the shell. The *H. neapolitanus* G42L pore mutant grew at a significantly slower rate than wild type in ambient air. The *H. neapolitanus* F40D pore mutant had a different growth rate to wild type *H. neapolitanus* cells in ambient air. Carboxysome were purified from both pore mutants and the polypeptide composition of the carboxysomes was compared using Western blots with antibodies specific for certain

carboxysomal polypeptides. Both mutant organelles had an increased amount of CsoS1D when compared to wild type carboxysomes. Electron micrographs of purified carboxysomes from each pore mutant and wild type were compared. The size and shape of mutant and wild type carboxysomes were compared by electron microscopy. Based on the results for the F40D and G42L mutant growth curves, changing the pore does appear to affect the function of the carboxysomes.

DEDICATION

I would like to dedicate this thesis to my family, especially my mom and granny, for all their support throughout my graduate career.

ACKNOWLEDGMENTS

I would like to thank my graduate advisors, Dr. Sabine Heinhorst and Gordon Cannon, and my other committee members, Dr. Vijay Rangachari, Douglas Masterson, and Faqing Huang, for their patience, advice, and guidance throughout my graduate career. I would also like to thank past and present graduate students of the Chemistry and Biochemistry Department at The University of Southern Mississippi (USM) for their guidance and friendship in and out of the lab, especially Evan Roberts, Dr. Balaraj Menon, Avijit Biswas, Fei Cai, Zhicheng Dou, and Scott Walper.

I would also like to thank the Biology Department (USM), especially the members of Dr. Glen Shearer's lab and Kenneth's Curry lab, which were always helpful. I appreciate the funding, patience, and guidance of the Principal Investigator, Co-Principal Investigators, and Director of the National Science Foundation (NSF) GK-12 Program at USM "Connections in the Classroom: Molecules to Muscles" #0947944, Dr. Sarah Morgan, Sabine Heinhorst, Sherry Herron, Jeffrey Wiggins, Richard Mohn, and Kimberly Wingo, respectively. I would also like to thank NSF Molecular and Cellular Biosciences (MCB) #0818680 and Graduate Assistantship in Areas of National Need (GAANN) for their funding.

TABLE OF CONTENTS

LIST OF ILLUSTRATIONS

Figure

LIST OF ABBREVIATIONS

β-ME	2-mercaptoethanol
APS	ammonium persulfate
BCA	bicinchoninic acid
Bicine	N,N-Bis(2-hydroxyethyl)glycine
BMC	bacterial microcompartment
bp	base pair
BSA	bovine serum albumin
CA	carbonic anhydrase
CCM	carbon dioxide concentrating mechanism
CBB	Calvin-Benson-Bassham
Ci	inorganic carbon
CIAP	calf intestinal alkaline phosphatase
CO_2	carbon dioxide
DIC	dissolved inorganic carbon
DTT	dithiothreitol
EtOH	ethanol
HCR	high CO_2-requiring
HRP	horseradish peroxidase
IgG	immunoglobulin G
IPTG	isopropyl-β-D-thiogalactoside
MES	2-(N-morpholino)ethanesulfonic acid
MOPS	3-(N-morpholino)propanesulfonic acid

NADH	nicotinamide adenine dinucleotide
NADP	nicotinamide adenine dinucleotide phosphate
NBT	4-nitroblue tetrazolium
NTA	nitrilotriacetic acid
OD	optical density
PAGE	polyacrylamide gel electrophoresis
PBS	phosphate-buffered saline
PCR	polymerase chain reaction
PG	2-phosphoglycolate
PGA	3-phosphoglycerate
PMSF	phenylmethylsulfonyl fluoride
PTSF	p-toloenesulfonyl fluoride
RubisCO	ribulose 1,5-bisphosphate carboxylase/oxygenase
RuBP	ribulose 1,5-bisphosphate
SDS	sodium dodecyl sulfate
TEM	transmission electron microscopy
TEMED	N,N,N',N'-Tetramethylethylenediamine
TEV	tobacco etch virus
Tris	Tris-(hydroxymethyl)-aminomethane base

CHAPTER I

INTRODUCTION

For many decades, it was believed that prokaryotes lacked specialized organelles. In 1973, prokaryotic organelles called carboxysomes were discovered in chemoautotrophic bacteria called *Halothiobacillus neapolitanus*.[1] All cyanobacteria and some chemoautotrophs produce carboxysomes that aid in CO_2 fixation. The carboxysomes encapsulate ribulose 1,5-bisphosphate carboxylase/oxygenase (RubisCO, EC 4.1.1.39), a key enzyme in the Calvin-Benson-Bassham cycle. RubisCO fixes CO_2 onto the backbone of ribulose 1,5-bisphosphate (RuBP) to form two molecules of 3-phosphoglycerate (3-PGA).[1-3] RubisCO is a catalytically inefficient enzyme that binds poorly to its substrates. Autotrophic organisms have evolved a way to compensate for the low catalytic efficiency of RubisCO by utilizing a mechanism known as the CO_2-Concentrating Mechanism (CCM).[4] RubisCO also catalyzes the fixation of O_2, which produces a wasteful byproduct at the expense of ATP and reducing agents.[5-7] The initial role of this mechanism is to concentrate intracellular bicarbonate.[2,3,8] The final step of the CCM involves the RubisCO and carboxysomal carbonic anhydrase enzymes.[9] The shell-associated carbonic anhydrase is responsible for the rapid equilibration of bicarbonate and carbon dioxide within the carboxysome. It is speculated that the carboxysome shell impedes the diffusion of CO_2 out of the carboxysome and, therefore, elevates the concentration of CO_2 in the carboxysome, which is immediately fixed by carboxysomal RubisCO.[10]

A model organism for this study is the chemoautotroph, *Halothiobacillus neapolitanus*, due to the successful recovery of functional carboxysomes.[9] The

carboxysome is made up entirely of proteins. The carboxysomal RubisCO is comprised of two subunits: CbbL and CbbS. The remaining proteins that make up the carboxysome are shell components CsoS2A, CsoS2B, CsoSCA, CsoS4A, CsoS4B, CsoS1C, CsoS1A, CsoS1B, and CsoS1D. CsoS1 has four paralogs: CsoS1A, CsoS1B, CsoS1C, and CsoS1D.[11] The carboxysomal shell proteins, the CsoS1A, B, and C paralogs, are the most prominent shell proteins that form the flat molecular layer of the polyhedral facets. CsoS1D forms pseudohexamers that have been shown to be a shell component but at a lower abundance when compared to CsoS1A, B, and C hexamers.[12] The minor shell proteins, CsoS4A and CsoS4B, form the pentamer vertices of the carboxysome shell.[13] CsoS2A and CsoS2B are shell-associated but the structure and function has not been determined.[14] The carboxysomal shell carbonic anhydrase, CsoSCA, is responsible for interconversion of cytosolic bicarbonate into carbon dioxide.[8,15,16]

It is currently unknown how the negatively charged RubisCO metabolites diffuse across the carboxysome shell. It is believed that the carboxysome shell acts as a diffusion barrier for RubisCO metabolites.[8] The carboxysome shell is mostly comprised of CsoS1 hexamers. The CsoS1 hexamers have a small central pore that is about 4 Å in diameter.[17] It is speculated that the central pore of the CsoS1 hexamers plays a role in the diffusion of RubisCO metabolites. The slightly positive surface potential of the central pore may allow for negatively charged RubisCO metabolites to cross the shell.[15]

The carboxysome assembly pathway as well as the role of the carboxysome shell in enhancing the catalytic efficiency of RubisCO is not well understood. Even though many carboxysomal proteins have been discovered over the years, how the carboxysomal proteins assemble to form the functional carboxysome remains unclear. Understanding

protein assembly requires elucidating the interactions between different carboxysomal proteins. Discovering the protein interactions within the carboxysome may shed light on how the shell contributes to the CO_2 Concentrating Mechanism (CCM). There are two substructures within the carboxysome: the RubisCO core and the shell. Currently, the types of interactions that exist between the two substructures have not been completely elucidated. To investigate the protein interactions between RubisCO and specific carboxysome shell proteins and between the different shell proteins themselves, yeast two-hybrid studies were conducted by Eric Williams.[18] There are drawbacks to studying protein interactions using the yeast two-hybrid system. Since these proteins are expressed in yeast, the amount of protein expression will be different than the expression level of the proteins within *H. neapolitanus*. In addition, the yeast two-hybrid system only reports protein interactions of just two proteins at a time and therefore cannot determine if additional proteins are needed for protein complexes to form. Another technique such as a pull-down assay may be an alternative route in discovering the assembly pathway of the carboxysomes without the drawbacks of the yeast two-hybrid system. A pull-down assay is an invaluable technique by which multiple interacting protein partners can be analyzed. This method is a form of *in vitro* affinity purification that uses a tagged protein (bait) that binds to its partner (prey), forming a protein complex that can be purified.

The goal of this study was to provide the first steps in understand the role of the carboxysome shell and the assembly pathway of the carboxysome in enhancing the catalytic efficiency of RubisCO.

CHAPTER II

LITERATURE REVIEW

Halothiobacillus neapolitanus

Halothiobacillus species are obligate aerobic bacteria that can live in sulfur-containing environments such as marine, freshwater, sulfur springs, sulfur deposits, sewage-treatment areas, etc.[19] *Halothiobacillus neapolitanus* is a chemoautotroph that plays an important role in the geochemical carbon and sulfur cycles by relying completely on reduced sulfur compounds and inorganic carbon dioxide to satisfy its energy and carbon needs, respectively.[20] Its role in the sulfur cycle involves oxidizing reduced sulfur compounds such as sulfide, thiosulfate, and inorganic sulfur to produce sulfate inside the cell.[18] The sulfur oxidation scheme illustrates the oxidization steps that thiosulfate undergoes inside and outside the cell (Figure 1). Thiosulfate is relatively unstable at low pH and may degrade into sulfur *(h)* and sulfide *(i)*.[18,21,22] Sulfide enters the cell using an ATP-binding cassette transporter *(i)* and is oxidized to elemental sulfur *(a)*. The cytosolic sulfur undergoes an enzymatic condensation with sulfite to produce thiosulfate *(b)*. The thiosulfate is then oxidized to tetrathionate *(c)*. The tetrathionate has two fates: remain in the cell and is oxidized into trithionate *(d)* or exit the cell to give rise to trithionate and pentathionate *(g)*. The first fate results in the pentathionate undergoing an inorganic reaction producing tetrathionate and elemental sulfur *(h)*. The second fate results in the production of sulfite *(e)* from trithionate and finally produces sulfate *(f)*. Both trithionate and tetrathionate can be present in the bacterial media for several hours. The extracellular sulfur produced is insoluble making the media cloudy but will eventually be converted to sulfide which will be transporter into the cell *(i)*.

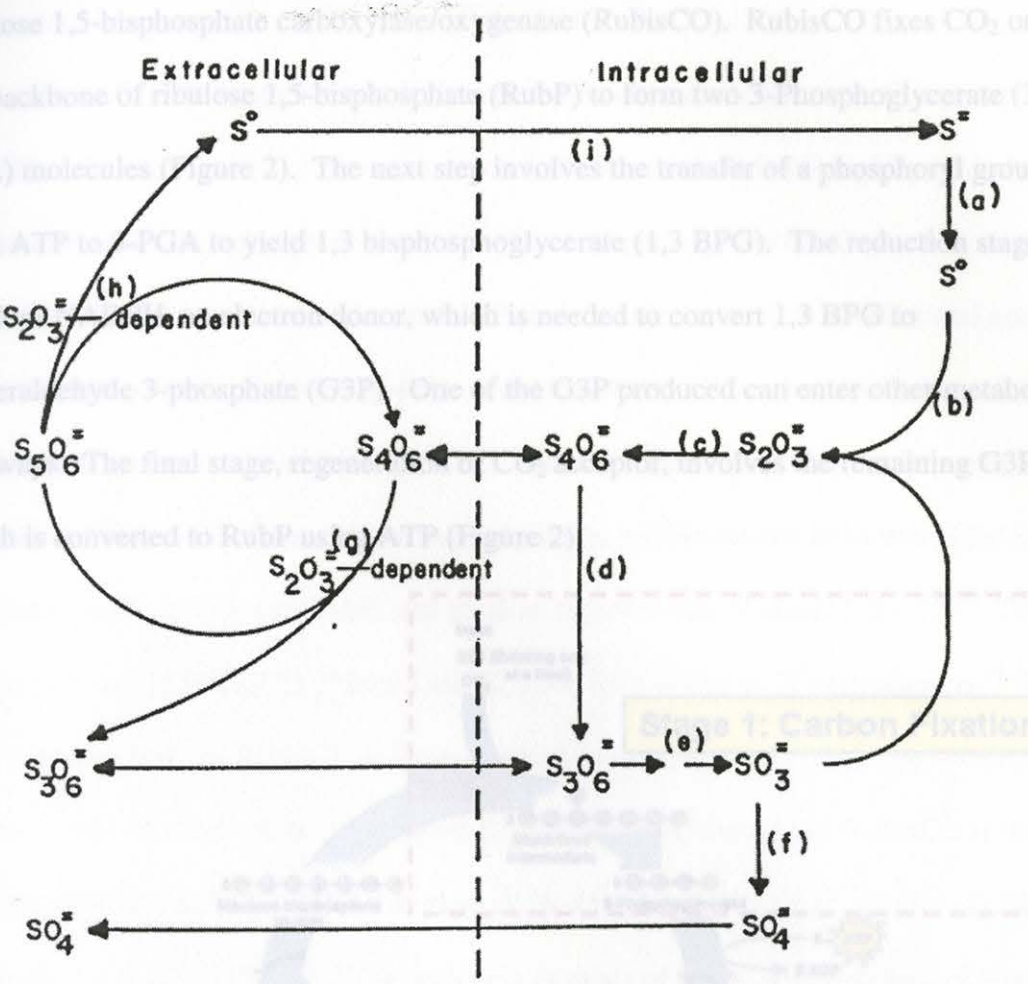

Figure 1. Sulfur Oxidation Scheme of *Halothiobacillus* sp. See text for explanation.[20]

To satisfy its carbon needs, *H. neapolitanus* utilizes the Calvin-Benson-Bassham cycle to convert atmospheric carbon dioxide into organic compounds. The Calvin-Benson-Bassham cycle uses the high-energy compound, ATP and the electron carrier, NADPH, to convert carbon dioxide and water into organic compounds that are needed for the organism to grow.[23] This cycle is utilized by many organisms such as plants, algae, cyanobacteria, phototrophic and chemoautotrophic bacteria. The Calvin-Benson-Bassham cycle consists of three stages: carbon dioxide fixation, reduction, and regeneration of the CO_2 acceptor (Figure 2). The key enzyme of this reaction pathway is

ribulose 1,5-bisphosphate carboxylase/oxygenase (RubisCO). RubisCO fixes CO_2 onto the backbone of ribulose 1,5-bisphosphate (RubP) to form two 3-Phosphoglycerate (3-PGA) molecules (Figure 2). The next step involves the transfer of a phosphoryl group from ATP to 3-PGA to yield 1,3 bisphosphoglycerate (1,3 BPG). The reduction stage involves NADPH, an electron donor, which is needed to convert 1,3 BPG to glyceraldehyde 3-phosphate (G3P). One of the G3P produced can enter other metabolic pathways. The final stage, regeneration of CO_2 acceptor, involves the remaining G3P which is converted to RubP using ATP (Figure 2).

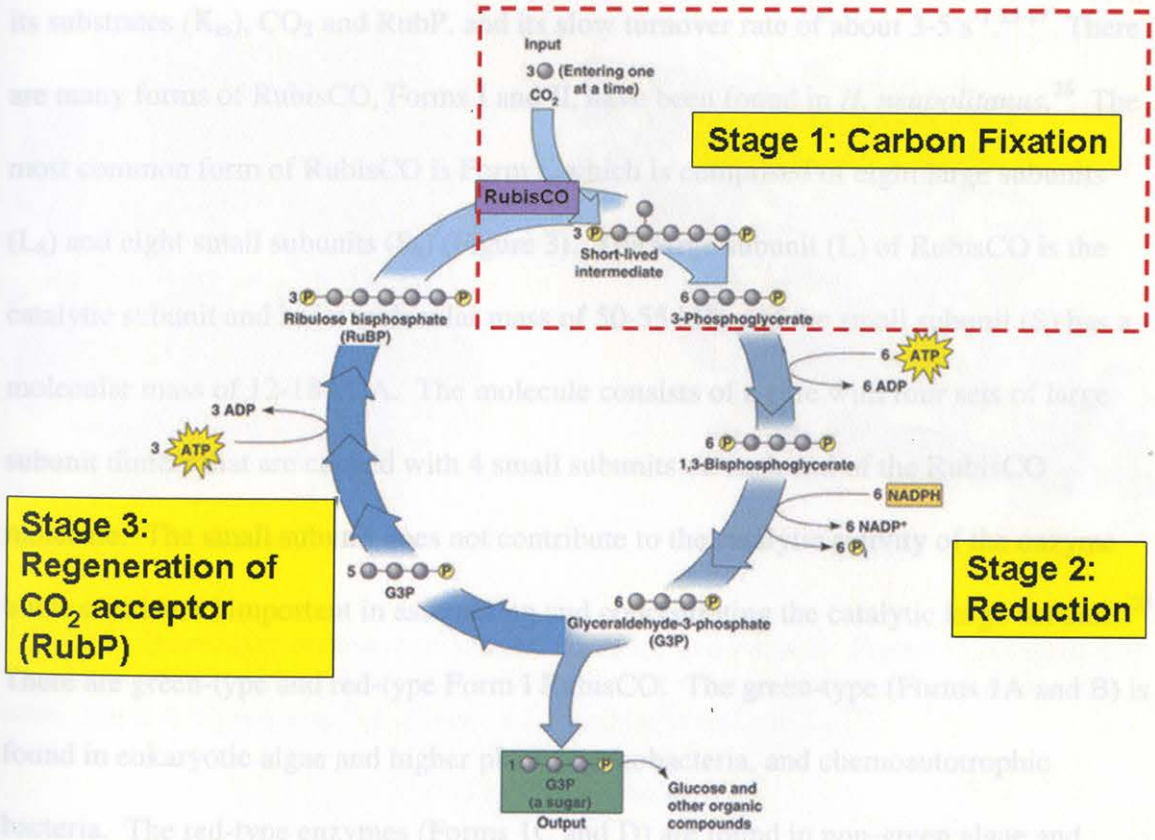

Figure 2. Calvin-Benson-Bassham Cycle. This cycle involves three main stages: CO_2 fixation of RuBP, reduction of 1, 3 BPG to G3P, and regeneration of RuBP.[24]

RubisCO

RubisCO fixes atmospheric CO_2 onto the backbone of ribulose 1,5-bisphosphate (RuBP), a 5-C molecule, to form an unstable 6-C intermediate that is rapidly hydrolyzed to two molecules of 3-phosphoglycerate (3-PGA) (Figure 2). RubisCO also has another substrate, O_2, which can be fixed onto RuBP to form one molecule of 3-PGA and one molecule of 2-phosphoglycolate (2-PG). Unlike 3-PGA, 2-PG is a wasteful byproduct that requires energy to convert it to 3-PGA. Although RubisCO is the primary enzyme in the Calvin-Benson-Bassham cycle, it is catalytically inefficient due to its low affinity for its substrates (K_m), CO_2 and RubP, and its slow turnover rate of about 3-5 s^{-1}.[25-27] There are many forms of RubisCO, Forms I and II, have been found in *H. neapolitanus*.[28] The most common form of RubisCO is Form I, which is comprised of eight large subunits (L_8) and eight small subunits (S_8) (Figure 3). The large subunit (L) of RubisCO is the catalytic subunit and has a molecular mass of 50-55 kDa and the small subunit (S) has a molecular mass of 12-18 kDA. The molecule consists of a core with four sets of large subunit dimers that are capped with 4 small subunits on each end of the RubisCO molecule. The small subunit does not contribute to the catalytic activity of the enzyme but is considered important in assembling and concentrating the catalytic large subunits.[25] There are green-type and red-type Form I RubisCO. The green-type (Forms 1A and B) is found in eukaryotic algae and higher plants, cyanobacteria, and chemoautotrophic bacteria. The red-type enzymes (Forms 1C and D) are found in non-green algae and phototrophic bacteria. Form II RubisCO, CbbM, are dimers of large subunits $(L_2)_n$ and do not contain the small subunit (Figure 3). Form II RubisCO has a lower affinity for its substrates when compared to the other forms of RubisCO. This may be due to the lack of

small subunits present in the holoenzyme of Form II.[29,30] This form of RubisCO is found in purple non-sulfur bacteria, several chemoautotrophic bacteria, and eukaryotic dinoflagellates. Some bacteria such as *Hydrogenovibrio marinus*, *Rhodobacter sphaeoides*, *R. capsulatus*, and several *Thiobacillus crunogena* contain both forms of RubisCO. The expression levels of the different forms of RubisCO vary at different concentrations of CO_2.[31] In the species *marinus*, Form II RubisCO is expressed at higher levels in elevated levels of CO_2.[31] This reveals a complicated regulatory mechanism involved in expression of the different forms of RubisCO.[31]

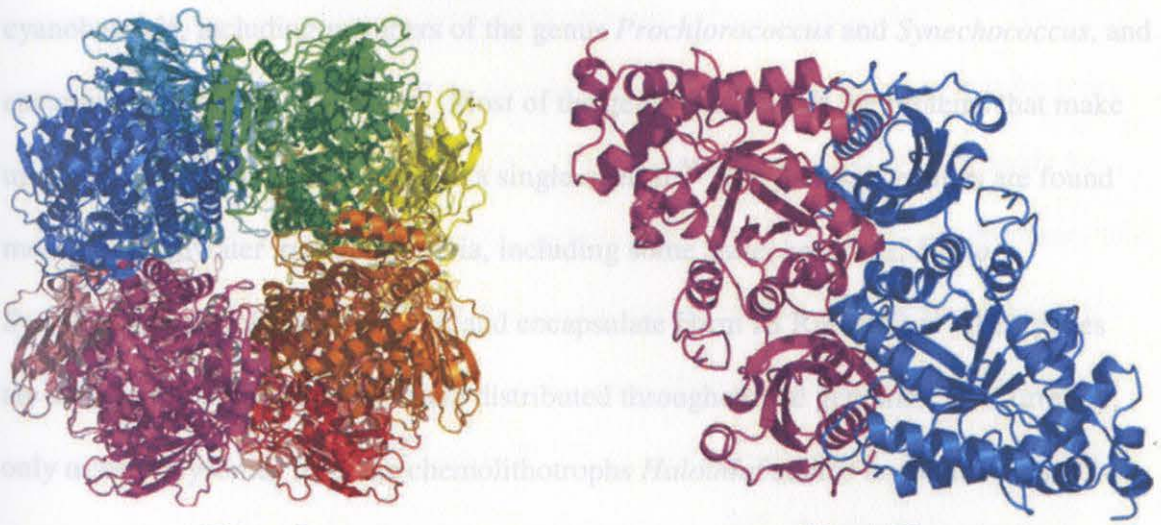

Figure 3. Quaternary Structure of RubisCO Form I and Form II. Form I is comprised of four large subunit dimers with small subunits on the top and bottom of the L_8 octameric core. Form II is comprised of dimers of L, ranging from L_2 to L_8.[25]

The Carboxysome

The carboxysome acts as proteinaceous bacterial organelle similar to the membrane-bound organelles in eukaryotes (Figure 4). Bacterial organelles, like eukaryotic organelles, provide advantages for the cell, such as housing and enhancing various metabolic processes. The icosahedral shape and symmetry of carboxysomes has

been compared to that of virions.[15] The α and β carboxysomes have a thin proteinaceous shell about 3-4 nm based on electron microscopic studies (Figure 4).[9,32] The carboxysome encapsulates several small granular particles called Form I RubisCO particles. Encapsulating RubisCO in the carboxysome shell is believed to enhance CO_2 fixation.[33-36]

There are two classes of carboxysomes, α and β, which are classified, based on gene arrangement, carboxysome composition, and encapsulated RubisCO. The α-carboxysomes which are generally found in chemolithotrophs and many marine cyanobacteria, including members of the genus *Prochlorococcus* and *Synechococcus*, and encapsulate Form 1A RubisCO.[37] Most of the genes that encode the proteins that make up the α-carboxysome are located in a single operon.[38] The β-carboxysomes are found mostly in freshwater in cyanobacteria, including some S*ynechococcus*, *Nostoc*, *Synechocystis, Trichodesmium,* etc. and encapsulate Form IB RubisCO.[33] Their genes are arranged in multiple clusters and distributed throughout the genome.[37,38] Currently, only α- carboxysomes from the chemolithotrophs *Halothiobacillus neapolitanus* and two strains of *Niterbacter*, as well as a cyanobacteria *Prochlorococcus* species, have been successfully purified and can be used for biochemical analysis.[9,32,39,40]

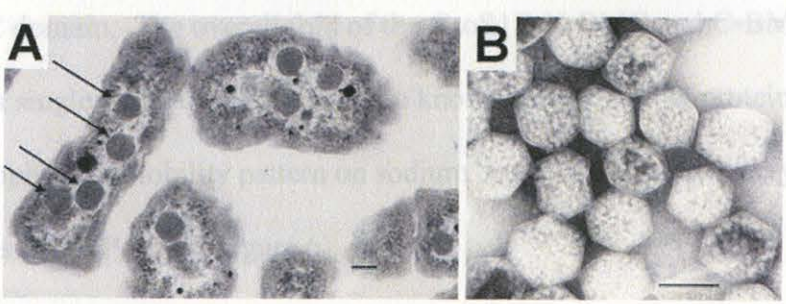

Figure 4. Negatively Stained Thin Sections of *H. neapolitanus* and Negatively Stained TEM of Carboxysomes. *(A)* Negatively stained thin sections of *H. neapolitanus* containing carboxysomes shown with arrows. *(B)* Negatively stained TEM showing the polyhedral structure of the carboxysome.[17]

The genes that encode most of the proteins that make up the α carboxysome are located in a single operon called *cso* operon. The genes are transcribed in this order: *cbbL*, *cbbS*, *csoS2*, *csoS3*, *csoS4A*, *csoS4B*, *csoS1C*, *csoS1A*, and *csoS1B* (Figure 5). Starting from the 5' end of the *cso* operon, the first set of genes, *cbbL* and *cbbS*, encodes the proteins that make up the holoenzyme, Form IA RubisCO (Figure 5). [30,41] The six remaining genes have been shown to be shell components.[9,42] The *csoS2* gene encodes two proteins, CsoS2A and CsoS2B. Currently, the structure and function of CsoS2A and CsoS2B have not been established.[14,43] The next gene in the operon is *csoS3* which encodes the protein that forms a dimer with carbonic anhydrase activity.[10,15,16] The *csoS4A* and *csoS4B* genes encode the protein that makes up the pentamers that form the vertices of the polyhedral carboxysomes.[13] The three remaining genes that encode the major shell proteins are *csoS1A, csoS1B,* and *csoS1C.* These proteins form hexamers that tile together to make the facets of the polyhedral carboxysome. The CsoS1 proteins are characterized as small domains known as Bacterial Microcompartment (BMC) domains and consists of ~90 amino acid residues.[44] The *csoS1D* gene is located outside the *cso* operon and encodes proteins that form pseudohexamers.[12,44] The CsoS1D protein is characterized as a double BMC domain due to the presence of an N-terminal and C-terminal BMC domain. The overall fold of the CsoS1D N-BMC and C-BMC is similar to the fold of a single BMC domain.[44] All the known carboxysomal proteins possess a distinct electrophoretic mobility pattern on sodium dodecyl sulfate-polyacrylamide gel electrophoresis (SDS-PAGE) (Figure 6).

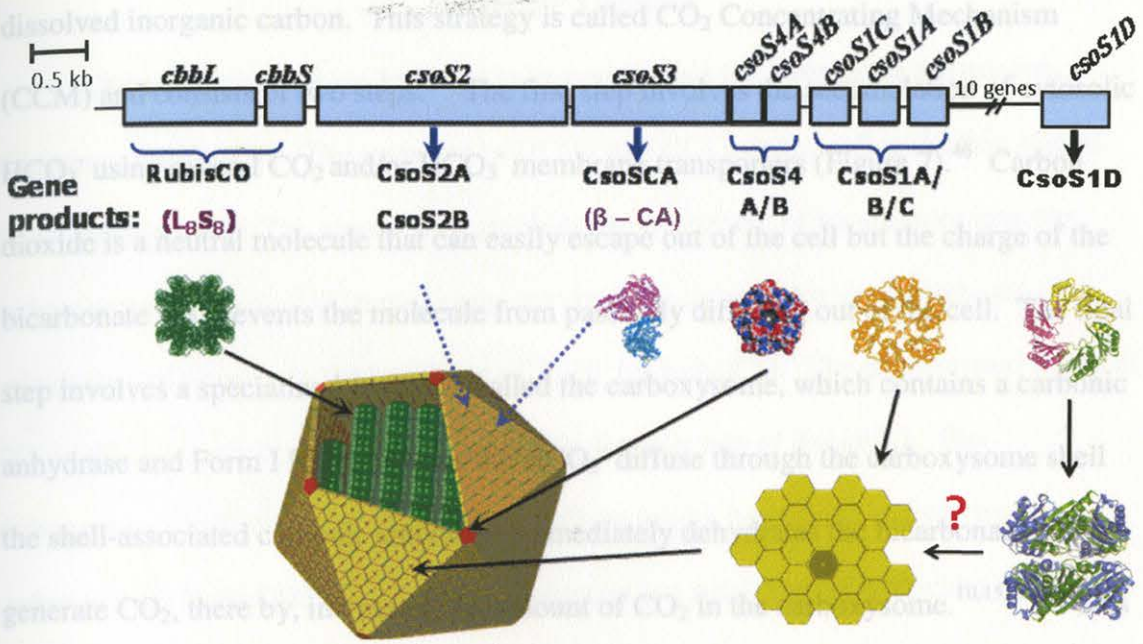

Figure 5. The Preliminary Atomic Model for α-Carboxysomes. The *cso* operon includes the first nine genes and is transcribed from left to right and starts with the large and small subunit of RubisCO and the remaining seven genes encode the proteins that make up the carboxysome shell. An additional *cso* gene, *csoS1D,* is located 10 genes downstream of the *cso* operon.[45]

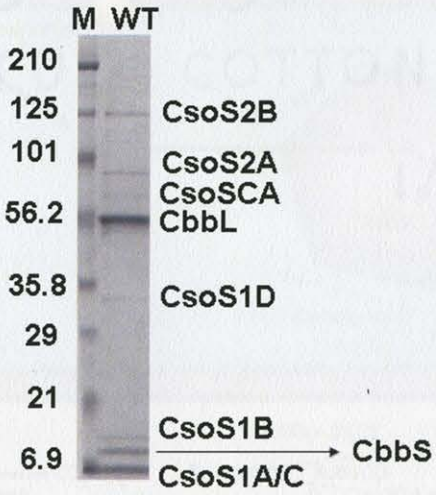

Figure 6. Purified Wild Type Carboxysome Polypeptides Separated by (SDS-PAGE). M=SDS-PAGE Prestained Protein Marker (kDa). WT= Polypeptides of purified *H. neapolitanus* carboxysomes.

CO_2 Concentrating Mechanism (CCM)

All cyanobacteria and some chemoautotrophs have adapted to the limited amounts of CO_2 in the environment by using an effective strategy that allows them to concentrate

dissolved inorganic carbon. This strategy is called CO_2 Concentrating Mechanism (CCM) and consists of two steps.[46] The first step involves the accumulation of cytosolic HCO_3^- using several CO_2 and/or HCO_3^- membrane transporters (Figure 7).[46] Carbon dioxide is a neutral molecule that can easily escape out of the cell but the charge of the bicarbonate ion prevents the molecule from passively diffusing out of the cell. The final step involves a specialized organelle called the carboxysome, which contains a carbonic anhydrase and Form I RubisCO. As the HCO_3^- diffuse through the carboxysome shell the shell-associated carbonic anhydrase immediately dehydrates the bicarbonate to generate CO_2, there by, increasing the amount of CO_2 in the carboxysome.[10,15,16,34] This mechanism ensures that CO_2 is fixed more efficiently by the encapsulated of Form I RubiscO.[33-36]

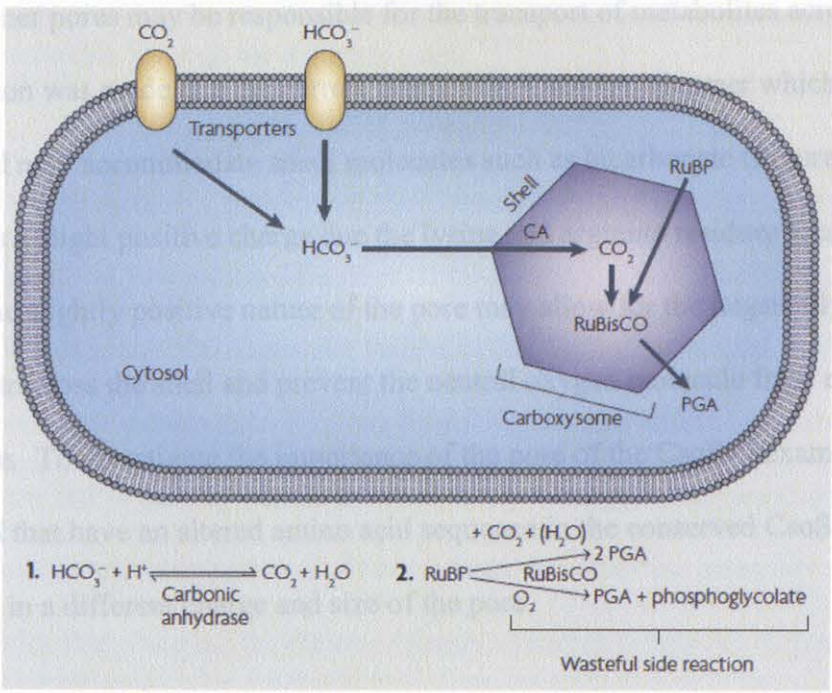

Figure 7. CO_2 Concentrating Mechanism (CCM). Step 1, the accumulation of cytosolic bicarbonate in the cell using membrane-bound transporters. Step 2, involves the carboxysome in which bicarbonate is converted to carbon dioxide by the shell-associated carbonic anhydrase which is then fixed by carboxysomal RubisCO.[47]

Metabolite Transport

The carboxysomes are believed to be responsible for optimizing the catalytic efficiency of RubisCO. The transport of HCO_3^- and CO_2 into the cell is the first step of the CCM (Figure 7). The second step involves the movement of bicarbonate into the carboxysome in which it is immediately converted to carbon dioxide by carbonic anhydrase and fixed onto the backbone of RuBP by RubisCO. The concentrated levels of CO_2 within the carboxysome increase the CO_2 fixation rate of RubisCO. The carboxysome shell may limit the passage of O_2 to inhibit oxygenase activity by carboxysomal RubisCO.[43] The RubisCO enzyme is a catalytically inefficient enzyme and can undergo carboxylation or oxygenation of the substrate, RuBP. It is believed that the carboxysome shell acts as a diffusion barrier for RubisCO metabolites and that the CsoS1 hexamer pores may be responsible for the transport of metabolites across the shell. This prediction was made due the narrow pore of the CsoS1A hexamer which is about 4-5 Å wide and may accommodate small molecules such as bicarbonate (Figure 8).[17] The pore also has a slight positive charge due the lysine and arginine residues located within the pore. The slightly positive nature of the pore may allow for the negatively charged bicarbonate to cross the shell and prevent the neutral oxygen molecule from entering the carboxysome. To investigate the importance of the pore of the CsoS1 hexamers, mutants were created that have an altered amino acid sequence in the conserved CsoS1 pore motif that resulted in a different charge and size of the pore.

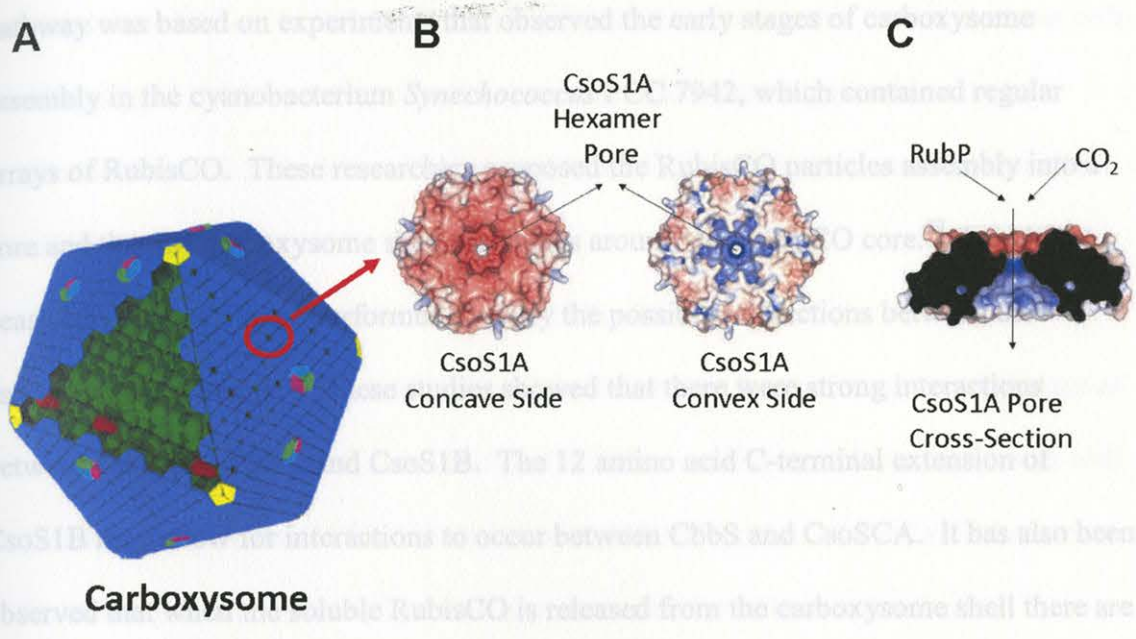

Figure 8. The Preliminary Atomic Model for the Carboxysome and an Electrostatic Comparison of the CsoS1A Hexamer. *(A)* Three dimensional image of the carboxysome *(B)* The images are electrostatic comparisons of the different sides of the CsoS1A. The red color indicates a negative surface potential and the blue represents a positive surface potential. *(C)* Pore cross-section of the CsoS1A hexamer and the predicted diffusion of RubisCO metabolites through the hexamer pore.[17,48]

Shell Assembly

The overall assembly pathway of the carboxysome shell is still unknown despite the knowledge of the structure and function of the carboxysomes. Earlier studies suggested possible interactions between RubisCO and the carboxysomal shell based on electron microscopic studies that observed RubisCO particles within the carboxysome were tightly packed in paracrystalline arrays.[49,50] Previously, it was proposed that there were two possible assembly pathways of carboxysomes. The first assembly pathway was based on studies that observed the different stages of carboxysome development in thin sections of the cyanobacterium *Anabaena variabilis*.[51] Based on that research, it was proposed that the carboxysome shell assembles first, and that the carbonic anhydrase and RubisCO particles are inserted through the existing shell.[51] The other proposed assembly

pathway was based on experiments that observed the early stages of carboxysome assembly in the cyanobacterium *Synechococcus* PCC 7942, which contained regular arrays of RubisCO. These researchers proposed the RubisCO particles assembly into a core and that the carboxysome shell assembles around the RubisCO core.[52] In our lab, yeast 2-hybrid tests were performed to study the possible interactions between the carboxysomal proteins.[18] These studies showed that there were strong interactions between CsoSCA, CbbS, and CsoS1B. The 12 amino acid C-terminal extension of CsoS1B may allow for interactions to occur between CbbS and CsoSCA. It has also been observed that when the soluble RubisCO is released from the carboxysome shell there are some RubisCO molecules that remain with the shell.[18] CsoS1B may also associate with the small subunit of RubisCO to the carboxysome shell. A more direct method was developed to test the involvement of RubisCO in the biogenesis of carboxysomes by creating a mutant in which the genes that encode the proteins that Form I RubisCO are replaced with a kanamycin cassette in the genome of *h. neapolitanus*. This experiment determined that the remaining carboxysome proteins can assemble into a polyhedral shell without encapsulating RubisCO.[53] Further investigation is needed to determine the exact protein interactions within the carboxysome shell. Studying supramolecular complexes of the carboxysome may shed light on the role of the carboxysome shell in the CCM. To study the interactions within the carboxysome shell, the major CsoS1 carboxysome shell proteins were fused with a hexahistidine (His_6) tag that could allow for whole carboxysomes to be affinity purified. The His_6-tagged carboxysome may allow for further studies involving the identified of protein binding partners within the carboxysome. This may be accomplished by slightly denaturing the His_6-tagged

carboxysomes while it is on an affinity column and the proteins that do not associate with the His_6-tagged CsoS1 paralogs may be removed. The remaining proteins may be purified and identified to determine the protein binding partners that are formed with the CsoS1 paralogs.

Objective of the Study

The goal of this study was to provide a foundation for the future investigations of the importance of the carboxysome shell in the diffusion of RubisCO metabolites as well as the assembly pathway of the carboxysome and the orientation of the CsoS1 hexamers of the carboxysome. To investigate the importance of the carboxysome shell in metabolite diffusion, the CsoS1A hexamer pores were examined by changing either the size or charge. The growth characteristics of *H. neapolitanus* mutant cultures were studied, as well as the structure and composition of the carboxysomes produced by these mutants. It was determined that changing in the CsoS1A hexamer pores possibly hindered the metabolic flux of molecules across the shell, resulting in a high CO_2-requiring phenotype (HCR). To determine the assembly pathway of the carboxysomes, the three major shell components, CsoS1A, B, and C, were examined. Discovering the protein(s) that interact with the major shell paralogs may be important in understanding how the carboxysome shell enhances the catalytic efficiency of RubisCO. Therefore, the generation of His_6-tagged CsoS1 paralogs may be important in studying the interacting protein partners that form the functional carboxysome and the orientation of the CsoS1 hexamers in the carboxysome shell.

CHAPTER III

EXPERIMENTAL PROCEDURES

Routine Material

Routine materials and chemicals were purchased from Sigma, VWR, and Fisher Science. Criterion PreCast 4-20% polyacrylamide gradient Tris-HCl protein gels, PreCast 10-20% polyacrylamide gradient Tris-HCl protein gels, 40% polyacrylamide/Bis 29:1 (3.3% C), Prestained SDS-PAGE Standards, Broad Range, BCA protein assay reagents, and nitrocellulose blotting paper were purchased from BioRad. One-Step NBT-BCIP reagent, GelCode Blue, 2 mg/ml BSA protein standard, Modified Lowery Assay Kit, and B-PER II were purchased from Thermo Scientific. Oligonucleotides were acquired from Integrated DNA Technology (IDT). Restriction Enzymes, Deep Vent DNA Polymerase, and DNA Ligase were purchased from New England BioLabs. Deoxynucleotide triphosphate (dNTPs) mixture was acquired from Takara Bio Inc. Plasmid Isolation kits and Gel DNA Recovery Kits were purchased from Qiagen and Zymo Research. Rabbit anti-CsoS1 polyclonal antibodies, Rabbit anti-CsoSCA polyclonal antibodies, Rabbit anti-CsoS1D polyclonal antibodies, Rabbit anti-CsoS2 polyclonal antibodies were generated at Cocalico Biologicals. Chicken anti-RbcL antibodies (product No. AS01017) were purchased from Agrisera. Goat anti-chicken and Goat anti-rabbit HRP-tagged antibodies were acquired from Santa Cruz Biotechnology. Formvar/carbon coated 300 mesh copper grids, Kodak EM film 4489, and ammonium molybdate stain were purchased from Electron Microscopy Services.

Routine Apparatus

H. neapolitanus was grown in autotrophic liquid media inside an ATR Infors-HT Multitron shaker or maintained in an ATR Infors-HT labfors 2 L fermenter. Cultures were also grown in autotrophic media containing agar inside a 1572 or a Fisher Scientific Isotemp Plus D650 incubator. Cultures of *E. coli* were grown in Fisher Scientific Isotemp or an Eauatherm 1572 incubator, a New Brunswick TC-7 culture rotator, or a New Brunswick Series 25 incubator shaker. Long term storage of cultures, clones, and DNA was accomplished using Thermo Scientific Revco Elite series -80°C freezer. Sterilization of media and solutions were done in a Steris Amsco Lab 250 or a 3031-S autoclave. Protocols requiring sterile techniques were carried out in a SterilFuard Class II Type A/B3 hood by Baker Company Inc. Cell breaking was done using a Branson model 450 sonifier. Short-term storage of cellular extracts at 4°C was accomplished using a Sears or Whirlpool refrigerator. Optical density measurements were made in a Beckman Coulter DU800 UV-Vis Spectrophotometer. Large scale high speed centrifugations were carried out in Beckman Avanti J-301 and Avanti J-26XP centrifuges using the JLA-8.1, JA-14, JA-20, JLA-16.25, JSP-24.38 and F14BCI-6x250y series rotors, while microcentrifugation was done in an Eppendorf 5417C and 5417R microcentrifuge. Ultracentrifugation was performed in a Beckman L7-65 ultracentrifuge as well as a Beckman Optima Max ultracentrifuge. Polymerase Chain Reaction (PCR) for DNA amplification was run in BioRad's MyCycler thermal cycler. DNA restriction digests (37°C) and ligation reactions (16°C) were incubated in Fisher Versa-Bath model 137 and 133 water baths, respectively. DNA gel electrophoresis was done using electrophoresis cells by Continental Lab Protocols model 75.710 and GibcoBRL Horizon

58 Model 200. DNA concentration measurements were done using a Nanodrop ND-1000 spectrophotometer. Protein gel electrophoresis was performed using a BioRad Criterion or Mini-Protean III cell. Western Blotting was done using a BioRad Mini Trans-Blot or Criterion electrophoresis transfer cell. Visualization and image capturing of DNA and proteins gels and immunoblots were done using BioRad's VersaDoc Imaging System. For electron microscopy, Zeiss EM 100 and scanning of negative imaging was done using an Epson Perfection V700 Flatbed Photo scanner. Microliter volumes were measured and pipetted using Rainin Pipetman P-1000, P-200, P-20, P-10, and P-2 pipettes. For pipetting larger volumes, Drummond Pipet-aid, pH measurements were made by using an Orion 8102BNUWP Ross Ultra Combination pH probe connected to an Orion 720A+ pH meter from Termo Electron. Optical density measurements were made in a Beckman Coulter DU800 UV-vis spectrophotometer.

Bacterial Growth Media

Antibiotic Stock Solutions

100 mg/ml ampicillin in water (final concentration in LB medium is 100 μg/ml)

50 mg/ml kanamycin in water (final concentration in LB medium is 50 μg/ml)

34 mg/ml chloramphenicol in ethanol (final concentration in LB medium is 34 μg/ml)

Antibiotic solutions were sterilized by filtering through a 0.2 μm filter (Millipore). They were added to the sterile medium after cooling to 40°C.

Luria-Bertani (LB) Medium

10 g/L tryptone

5 g/L yeast extract

10 g/L NaCl

The medium was autoclaved for 20 minutes at 121°C and 15 psi.

Halothiobacillus neapolitanus liquid medium

4 g/L KH_2PO_4

4 g/L K_2HPO_4

0.4 g/L NH_4Cl

0.4 g/L $MgSO_4$

10 g/L $Na_2S_2O_3 \cdot 5H_2O$

10 ml/L trace element solution

4 ml/L 1% (m/v) phenol red solution if needed

The medium was adjusted to pH 6.8 with 1 M KOH if needed, prior to autoclaving for 20 minutes at 121°C and 15 psi. For 8 L media, the autoclave time was increased to 90 minutes.

H. neapolitanus Solid Medium

0.2 g/L KH_2PO_4

0.8 g/L K_2HPO_4

0.01 g/L $CaCl_2$

1 g/L NH_4Cl

0.24 g/L $MgSO_4$

10 g/L $Na_2S_2O_3 \cdot 5H_2O$

15 g/L agar

1 ml/L trace element solution

4 ml/L 1% (m/v) phenol red solution

The medium was adjusted to pH 6.8 with 1 M KOH if needed, prior to autoclaving for 20 minutes at 121°C and 15 psi.

H. neapolitanus Trace Element Solution

50 g/L EDTA

5.44 g/L $CaCl_2$

1.61 g/L $CoCl_2$

1.57 g/L $CuSO_4 \cdot 5H_2O$

4.99 g/L $FeSO_4 \cdot 7H_2O$

5.06 g/L $MnCl_2 \cdot 4H_2O$

1.10 g/L $(NH_4)6Mo_7O_{24} \cdot 4H_2O$

2.20 g/L $ZnSO_4 \cdot 7H_2O$

EDTA was dissolved in water first and the pH was brought to 6.0 with 20% (w/v) KOH. Next, the remaining chemicals were added sequentially as listed and the pH was adjusted to 6.0 with 20% (w/v) KOH. Finally, the pH was brought to 6.8 with 20% (w/v) KOH and the solution was stored at 4°C prior to use.

SOC Medium

20 g/L tryptone

5 g/L yeast extract

0.584 g/L NaCl

0.186 g/L KCl

0.952 g/L $MgCl_2$

1.204 g/L $MgSO_4$

3.603 g/L glucose

The medium was adjusted to pH 7.0 with 1 M KOH if needed, prior to autoclaving for 20 minutes at 121°C and 15 psi.

Buffers

6x DNA Gel-Loading Solution

0.25% (w/v) bromophenol blue

40% sucrose in water

Immunoblot Transfer Buffer

25 mM Tris-HCl (pH 8.3)

250 mM glycine

20% (v/v) methanol

Phosphate-Buffered Saline (PBS)

10 mM Na_2HPO_4

2 mM KH_2PO_4

137 mM NaCl

2.7 mM KCl

pH 7.4

Immunoblot Blocking Buffer

5% nonfat milk in PBS with 0.1% Triton X-100

Phenylmethylsulfonylfluoride (PMSF)/p-toluenesulfonylfluoride (PTSF) Stock Solution

100 mM PMSF/PTSF dissolved in 95% ethanol

Lysis Buffer (pProEX protocol)

50 mM Tris-HCl (pH 8.0 at 4°C)

5 mM 2-mercaptoethanol (added immediately before use)

1 mM PMSF/PRSF (added immediately before use)

Column Equilibration Buffer (modified pProEX protocol)

20 mM Tris-HCl (pH 8.0 at 4°C)

100 mM KCl

5 mM 2-mercaptoethanol (added immediately before use)

10% v/v Glycerol

20 mM Imidazole

High Salt Buffer (modified pProEX protocol)

20 mM Tris-HCl (pH 8.0 at 4°C)

500 mM KCl

5 mM 2-mercaptoethanol (added immediately before use)

10% v/v Glycerol

Elution Buffer (modified pProEX protocol)

20 mM Tris-HCl (pH 8.0 at 4°C)

500 mM KCl

5 mM 2-mercaptoethanol (added immediately before use)

10% v/v Glycerol

250 mM Imidazole

Protein Dialysis Buffer for Recombination Proteins

20 mM Bicine (pH 8.0)

400 µM PMSF/PTSF

1x SDS-PAGE Running Buffer (Laemmli)

25 mM Tris-HCl

192 mM glycine

1% w/v SDS

Western Blot Transfer Buffer at 4°C

25 mM Tris-HCl

192 mM glycine

20% v/v methanol

Immunoblot Blocking Buffer

5% non-fat dry milk in PBS buffer containing 0.1% v/v Triton X-100

4x SDS Gel-Loading Buffer

200 mM Tris-HCl (pH 6.8)

8% (w/v) SDS

0.4% (w/v) bromophenol blue

40% (v/v) glycerol

400 mM DTT or β-mercaptoethanol (β-ME)

1x TAE buffer

40 mM Tris-acetate (pH 8.3)

1 mM EDTA

1x TBE Buffer

89 mM Tris (pH 8.)

89 mM Boric acid

2 mM EDTA

TE Buffer

10 mM Tris-HCl (pH 8.0)

1 mM EDTA

BEMB Buffer

10 mM Bicine (pH 8.0)

1 mM EDTA

20 mM $MgCl_2$

20 mM $NaHCO_3$

Bacterial Strains

Halothiobacillus neapolitanus c2 (ATCC 23641)

Wild Type H. neapolitanus and H. neapolitanus csoS1A::G42L mutant and csoS1A::F40D mutant.

Genotype of E. coli Strains

DH5α: *F- 80dlacZM15 (lacZYA-argF) U169 recA1 endA1 hsdR17(rk-, mk+) phoA supE44 - thi-1 gyrA96 relA1.*

TOP10: *F- mcrA (mrr-hsdRMS-mcrBC) 80lacZM15 lacX74 recA1 ara139 (ara-leu)7697 galU galK rpsL (StrR) endA1 nupG.*

DY330: *W3110 ΔlacU169 gal490 λcI857 Δ(cro-bioA)* (W3110 is a substrain of *E. coli* K-12).

Methods

Halothiobacillus neapolitanus c2 (ATCC 23641)

Halothiobacillus neapolitanus cultures were maintained on solid media and as liquid cultures. For biochemical characterization, *H. neapolitanus* cells were grown in the bioreactor at 0.08 h-1 dilution rate at pH 6.4 and 30°C. Wild type cells of *H. neapolitanus* were grown in air with ambient levels of CO_2. The G42L and F40D pore mutants of *H. neapolitanus* were grown in CO_2-enriched air (5% CO_2). The concentration of O_2 is approximately 21% (v/v).

Escherichia coli

E. coli TOP10 and DH5α strains were maintained in liquid and on solid LB medium under the appropriate selection pressure at 37°C for cloning manipulation. The genetically engineered strain DY330 was grown at 30°C for homologous recombination *in vivo*.

Isolation of Genomic DNA from H. neapolitanus

A 50 ml culture of *H. neapolitanus* was grown to stationary phase and cells were centrifuged at 10,000 x g in JA 25.5 rotor for 10 minutes at 4°C. To remove the insoluble sulfur from the cell pellet, the cells were resuspended in 5 ml of TE and centrifuged at 10,000 x g in JA 25.5 rotor for 5 minutes at 4°C. The cells were resuspended carefully without disturbing the sulfur pellet in 1 ml of TE. The cell suspension was transferred to 15 ml glass conical tube. An additional 1 ml of TE was added to dilute the cell suspension. The following was added to the cell suspension: 100 µl of sterile 10% SDS solution, 20 µl of 10 mg/ml of Proteinase K, and 4 µl 10 mg/ml RNase A. The cell suspension was incubated at 37°C for 30 minutes until the solution was clear (all the cells were lysed). Saturated phenol was added slowly in a 1:1 ratio. The cell suspension was gently inverted several times until the solution turned cloudy. The cell suspension was centrifuged at 7,000 x g for 10 minutes at 4°C. After centrifugation the cell suspension was incubated at room temperature for 15 minutes or until the solution was clear. The aqueous layer which contained the genomic DNA was gently removed and placed in a new glass centrifuge tube without disturbing the phenol layer. A 0.1 volume of 3M NaAC pH 5.2 was added to the aqueous layer and gently mixed. Cold (-20°C) Isopropanol was slowly added in a 1:1 ratio to the aqueous layer containing the DNA. The aqueous layer was gently mixed, which allowed for the DNA to precipitate and formed a milky white clump. Using the P-1000 pipetman, the milky clump was

transferred to a small microfuge tube and centrifuge at 1,000 x g for 2 minutes to pellet the DNA. The supernatant was removed and the DNA pellet was resuspended in 70% cold EtOH. The microfuge tube was gently inverted several times and then centrifuged at 1,000 x g for 2 minutes. The EtOH rinse step was repeated two more times. The washed wet DNA pellet was transferred to a new microfuge tube and resuspended in 30 µl of TE or water. The genomic DNA was stored at -20°C.

Mini-Scale Plasmid DNA Preparation

A 3 ml broth culture of *E. coli* containing the plasmid of interest was grown overnight before harvesting. The cells were pelleted by centrifugation in a microfuge tube at 14,000 rpm for 2 minutes. The cell pellet was resuspended in 600 µl of H_20. The plasmid DNA from the cell suspension was extracted following the Zyppy Plasmid Miniprep Kit according to the manual.

Restriction Digest of Plasmid DNA

Plasmid DNA was digested with the appropriate restriction endonucleases in a total reaction volume of 10 µl. The reaction mixture included 200-500 ng of DNA, 1 µl of the appropriate 10 X digestion buffer, 1 µl of bovine serum albumin (10 mg/ml) if needed, and 10 units of each restriction endonuclease. The reactions were incubated in a 37°C water bath for 2 hours. The resulting DNA fragments were separated by agarose gel electrophoresis.

DNA Ligation

DNA ligation reactions were set up with a vector insert molar ratio of 1:3 or 1:5. The total reaction volume of 10 µl contained 100 ng of vector DNA, the corresponding amount of insert DNA, 1 µl of 10 X T4 DNA ligase buffer and 400-800 units of T4 DNA

ligase. The reaction was incubated in a 16°C water bath overnight. The reaction was used to transform chemically component *E. coli* cells.

Polymerase Chain Reaction (PCR)

Usually, 50 µl PCR reactions were set up in 0.3 ml thin-walled PCR tubes. Each reaction contained 1 X Taq buffer, 250 µM of each dNTP, 200 nM each of forward and reverse primer, 30 ng of plasmid DNA or 100 ng of genomic DNA as template, and 10 units of Deep Vent Polymerase. The thermal cycler was pre-heated to 95°C before inserting the PCR tubes. A typical PCR protocol consisted of an initial denaturation step at 95°C for 5 minutes, 25 repeat cycles of denaturation (95°C for 30 seconds), annealing (5°C below the melting temperature of the primers, 30 seconds), extension (72°C for 30-120 seconds, depending on the size of the region to be amplified, a final extension step at 72°C for 5 minutes, and a hold step at 4°C. If necessary, a temperature gradient was applied for the annealing step.

TOPO Cloning

The Zero Blunt TOPO PCR Cloning Kit was used to ligate PCR products into the PCR-Blunt TOPO vector. Typically, 3 µl of PCR product, 1 µl of salt solution, and 1 µl of TOPO vector were mixed and incubated for 30 minutes at room temperature. The reaction was used to transform chemically competent *E. coli* TOP10 cells.

Agarose Gel Electrophoresis for Separating and Visualizing DNA

DNA samples were prepared in 10 X agarose gel tracking dye and separated by electrophoresis on an agarose gel prepared in TBE buffer. The percentage of gel (0.8-2% w/v) depended on the size of the DNA to be separated. Electrophoresis was performed at 5 V/cm until the bromophenol blue dye reached half the length of the gel. The gel was

stained with 0.5 μg/ml ethidium bromide in water for 10 minutes and then rinsed in water for 30 minutes. The stained gel was placed on a UV transilluminator for visualization. Images were taken with a VersaDoc imaging system and Quantity One v 4.6.3 software. Stained bands of interest were excised from the gel with a clean razor. Gel slices were weighted and further processed using a Zymoclean Gel Recovery Kit.

Chemical Transformation of E. coli Cells

Either 10 ng of plasmid or 5 μl of ligation reaction was mixed with 55 μl of commercially available chemically component *E. coli* cells in pre-cold 10 ml round-bottom polystyrene tube, and incubated on ice for 30 minutes. Cells were heat shocked in a 42°C water bath for exactly 30 seconds and then immediately kept on ice for 2 minutes. A 200 μl aliquot of room temperature SOC medium was added to the cells and the suspension was incubated in a shaker at 300 rpm for 1 hour at 37°C. Aliquots of the cell suspension were plated on LB plates containing the appropriate antibiotic according to the resistance marker of the plasmid. The plates were incubated at 37°C overnight.

Electroporation of E. coli DY330 Cells

A saturated overnight DY330 culture was used as a 1:50 inoculation to generate a 50 ml subculture, and the subculture was incubated in the 30°C shaker at 300 rpm until the OD_{600} reading reached 0.5. Half of this culture was transferred into a sterile 250 ml baffled flask and incubated in a 42°C water bath with constant shaking for 15 minutes, while the remaining 25 ml culture was allowed to continue growing at 30°C as uninduced control. Both flasks were then transferred to an ice-water slurry, shaken to cool, and incubated for an extra 15 minutes. Cells were harvested by centrifuging at 8,000 rpm for 10 minutes at 4°C, and then resuspended in 1 ml of ice-cold sterile water. The cells

suspension was transferred to a 1.5 ml tube and centrifuged at 14,000 rpm for 20 seconds at 4°C. The supernatant was discarded, and the cell pellet was washed with 1 ml ice-cold sterile water. The wash step was repeated two more times. The final cell pellet was resuspended in 200 µl of ice-cold sterile water and kept on ice. For electroporation, 100 µl of induced or uninduced cells were mixed with 1 µg each of linear donor DNA and plasmid acceptor DNA, and then transferred into a 0.1 cm gap pre-cooled electroporation cuvette. Cells were electroporated at 2.0 kV, 25 µF with pulse controller set at 200 Ohms, and them immediately allowed to recover in 1 ml LB medium on ice for 5 minutes before incubation in a 30°C shaker for 1.5 hours. A 200 µl aliquot was plated on LB agar containing the appropriate antibiotic. Plates were incubated at 30°C overnight.

Electroporation of H. neapolitanus Cells

A 50 ml aliquot of exponentially growing *H. neapolitanus* cells was collected from the chemostat and harvested by centrifuging at 10,000 rpm in rotor JA25.5 for 10 minutes at 4°C. The cell pellet was resuspended in the same amount of ice-cold sterile water and centrifuged at 10,000 rpm at 4°C again. This step was repeated three more times to remove the salt from the cell suspension. The cell pellet was resuspended in 200 µl of ice-cold sterile water, and kept on ice. For electroporation, 60 µl of cells were mixed with 1 µg of plasmid DNA and then transferred into a 0.1 cm gap pre-cooled electroporation cuvette. Cells immediately recovered in 5 ml ice-cold *H. neapolitanus* media, and placed on ice for 5 minutes before incubating in the 30°C shaker with air supplemented with 5% CO_2. Cells were allowed to recover for 24 hours before adding 50 µg/ml of kanamycin, and then cultures were continuously incubated for 7 days until growth was observed. The cultures were also aliquotted onto low salt solid media

containing kanamycin. Only the colonies resistant to kanamycin were selected and analyzed by PCR amplification and genomic DNA sequencing.

Bicinchoninic Acid (BCA) Assay

Protein concentrations were determined using the Bicinchoninic acid assay. Duplicates were prepared for the standards and triplets were prepared for the sample. BCA protein assay reagent A and B were mixed with 50:1 ratio, and 950 µl of this mixture was distributed into each 1 ml plastic cuvette. One mg/ml BSA was used as standards, and 1 µg, 2 µg, 5 µg, 10 µg, 20 µg, and 40 µg were used to form a standard series. Two to ten microliters of sample was added into cuvette. Water was added for both standards and sample to adjust the volume to 1 ml. Reactions were incubated at 37°C for 30 minutes, and then they were mixed and read at a wavelength of 562 nm in DU 800 UV/vis spectrophotometer.

Mutant Generation

Generation of Pore Mutant Constructs

Based on the advice of collaborators, Drs. Cheryl Kerfeld and Fei Cai, specific amino acids were selected for altering the shape, charge, and diameter of the pore (Figure 15). The pore of the CsoS1A hexamer has the conserved motif sequence: phenylalanine (F), valine (V), glycine (G), glycine (G), glycine (G), and tyrosine (Y). The glycine (G) at the 42nd position of the CsoS1A monomer (V<u>G</u>GGY) was altered to a leucine (L) to create the G42L pore mutant and the other pore mutation altered the Phe40 (<u>F</u>VGGGY) to an aspartate (E) (Figure 9). Using the pHnHE-*csoS1A::G43A* plasmid (Figure 9B), which contains *csoS1A* site mutation, was amplified using Polymerase Chain Reaction (PCR) with a forward primer that annealed upstream of the desired mutation and a

reverse primer containing the desired mutation (Figure 9B). The resulting product was approximately 80 bp (Figure 9A). The 3' region of the *csoS1A* gene was amplified using a forward primer containing the desired mutation and a reverse primer that annealed on the 3' region of the *csoS1A* gene. The resulting product was approximately 170 bp (Figure 9A). Using overlapping PCR, the two previous PCR products were annealed together and amplified using the outermost 3' and 5' primers from two previous PCR reactions to create a full length PCR product. The final full length PCR product was approximately 250 bp and contained the desired mutation of the *csoS1A* gene (Figure 9C). The full length PCR product was digested with *Pml*I and *Bsu*36I endonucleases. The original pHnHE-*csoS1A::G43A* was also cut with the same enzymes. Using T4 ligase, the digested ~250 bp PCR product was ligated into the digested pHnHE-*csoS1A::G43A* plasmid (Figure 9C). Both mutations were created in the same way and they were named pHnHE::F40D and pHnHE::G42L plasmids. All plasmid constructs were confirmed by the University of Maine DNA Sequencing Facility in Orono, ME. All genomic DNA was confirmed by the SagaGene Company in Palo Alto, CA.

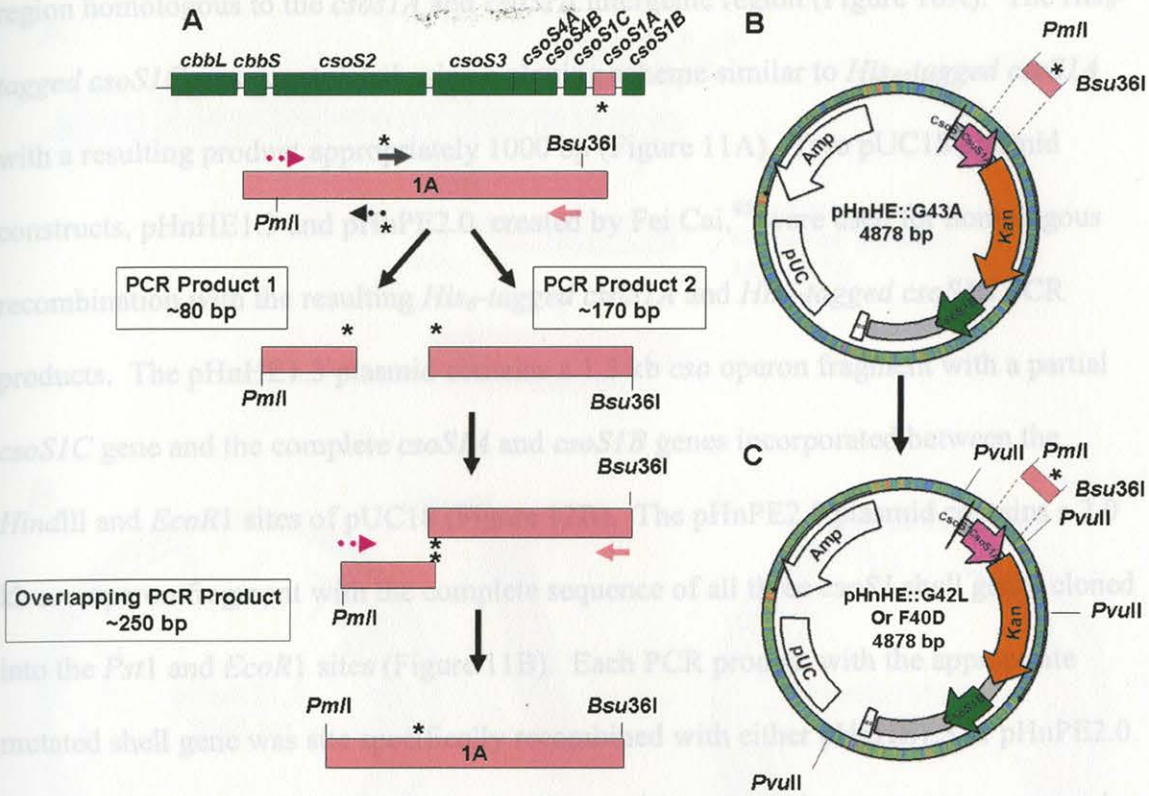

Figure 9. Generation of Pore Mutant Constructs. *(A)* The site-directed mutagenesis strategy for pore mutation plasmid constructs which involved amplifying *csoS1A* using primers containing the desired pore mutation. *(B)* pHnHE::G43A is a plasmid construct that contains *csoS1A* with G43 altered to alanine, *csoS1B*, and a kanamycin cassette located on the 5' end of *csoS1A* that was used to generate the pore mutation construct. Using T4 ligase, the digested ~250 bp Overlapping PCR product was ligated into the digested pHnHE-csoS1A::G43A plasmid to create pHnHE::F40D and pHnHE::G42L plasmids.

Generation of Plasmid Constructs that Encode C-terminally His_6-tagged CsoS1A and His_6-tagged CsoS1C

The following construction of His_6-tagged *csoS1A* plasmid was performed in order to investigate the expected protein interactions within the carboxysomal shell. An approximately 1000 bp fragment containing a kanamycin resistant cassette was constructed by PCR amplification with a forward primer containing a homologous region to the 3' region of *csoS1A* with a C-terminal His_6 tag and the 5' region of the kanamycin cassette and a reverse primer that annealed to 3' region of the kanamycin cassette and

region homologous to the *csos1A* and *csoS1B* intergenic region (Figure 10A). The *His$_6$-tagged csoS1C* was constructed using a cloning scheme similar to *His$_6$-tagged csoS1A* with a resulting product appropriately 1000 bp (Figure 11A). Two pUC18 plasmid constructs, pHnHE1.3 and pHnPE2.0, created by Fei Cai,[45] were used for homologous recombination with the resulting *His$_6$-tagged csoS1A* and *His$_6$-tagged csoS1C* PCR products. The pHnHE1.3 plasmid contains a 1.3 kb *cso* operon fragment with a partial *csoS1C* gene and the complete *csoS1A* and *csoS1B* genes incorporated between the *Hind*lll and *EcoR*1 sites of pUC18 (Figure 12B). The pHnPE2.0 plasmid contains a 2.0 kb *cso* operon fragment with the complete sequence of all three *csoS1* shell genes cloned into the *Pst*1 and *EcoR*1 sites (Figure 11B). Each PCR product with the appropriate mutated shell gene was site specifically recombined with either pHnHE1.3 or pHnPE2.0 in the DY330 strain of *Escherichia coli*. The resulting plasmid constructs were named pHnHE::1AH6-Kan and pHnHE::1CH6-Kan. To confirm the success of the homologous recombination reaction, the pHnHE::1AH6-Kan was digested with *Hind*III and *EcoR*I. The expected digestion pattern was approximately 2.2 kb and 2.7 kb (Figure 10C). The pHnPE::1CH6-Kan plasmid was digested with *Pst*I and *EcoR*I. The expected digestion pattern was approximately 2.9 kb and 2.7 kb (Figure 11C). The cloning scheme for each of the *His$_6$-tagged csoS1A* and *His$_6$-tagged csoS1C* plasmid constructs are outlined in Chapter IV. All plasmid constructs were confirmed by the University of Maine DNA Sequencing Facility in Orono, ME.

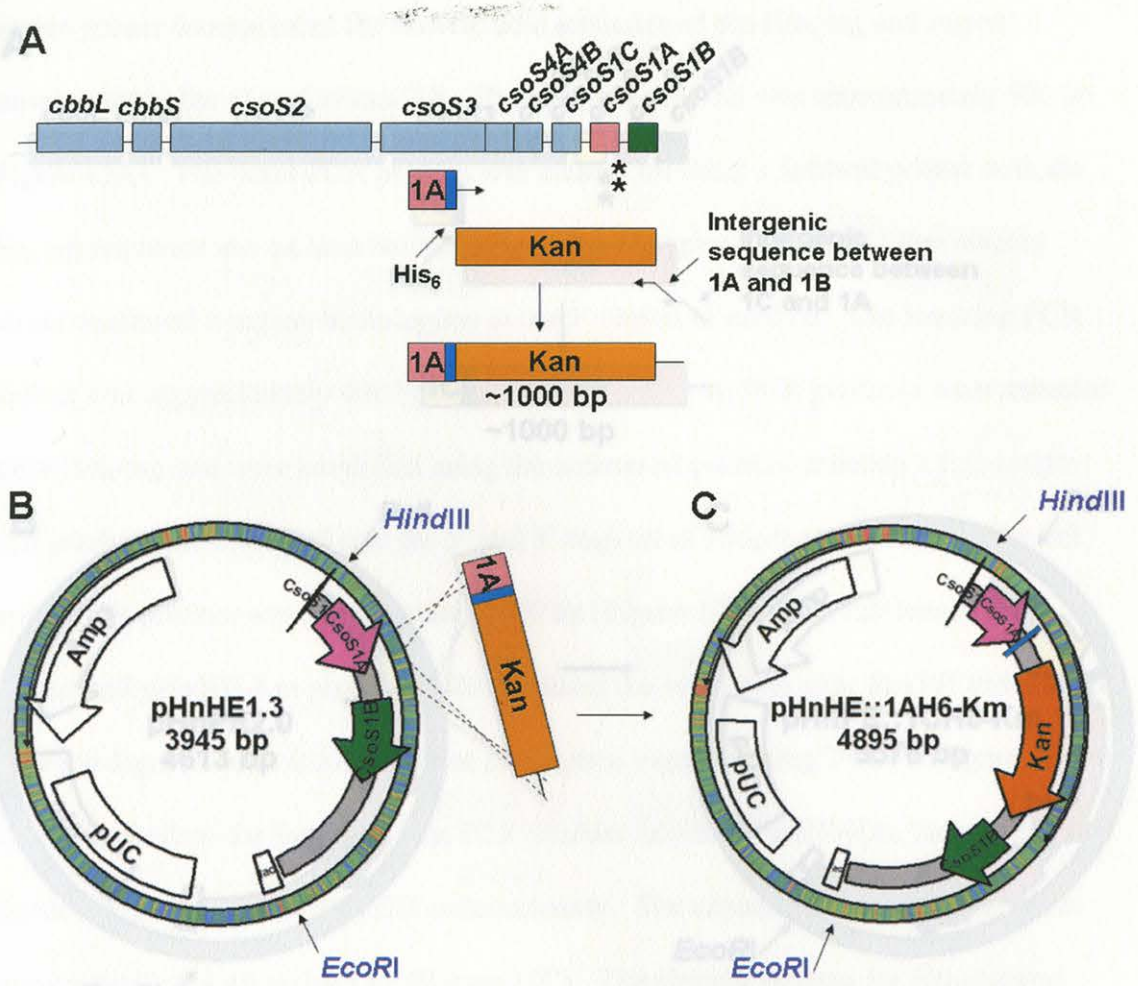

Figure 10. Strategy for Constructing pHnHE::1AH6-Km Plasmid. *(A)* PCR amplification strategy for the generation of a CsoS1A C-terminally His_6-tagged mutant. *(B)* pHnHE1.3 is a plasmid construct with a partial *csoS1C* and complete *csoS1A* and *csoS1B* genes within pUC18. *(C)* After recombination in *E. coli* DY330, the linear PCR fragments were incorporated into thepHnHE1.3 plasmid construct to create pHnHE::1AH6-Km plasmid construct. The asterisk represents the site in genome of *H. neapolitanus* in which the mutation will occur.

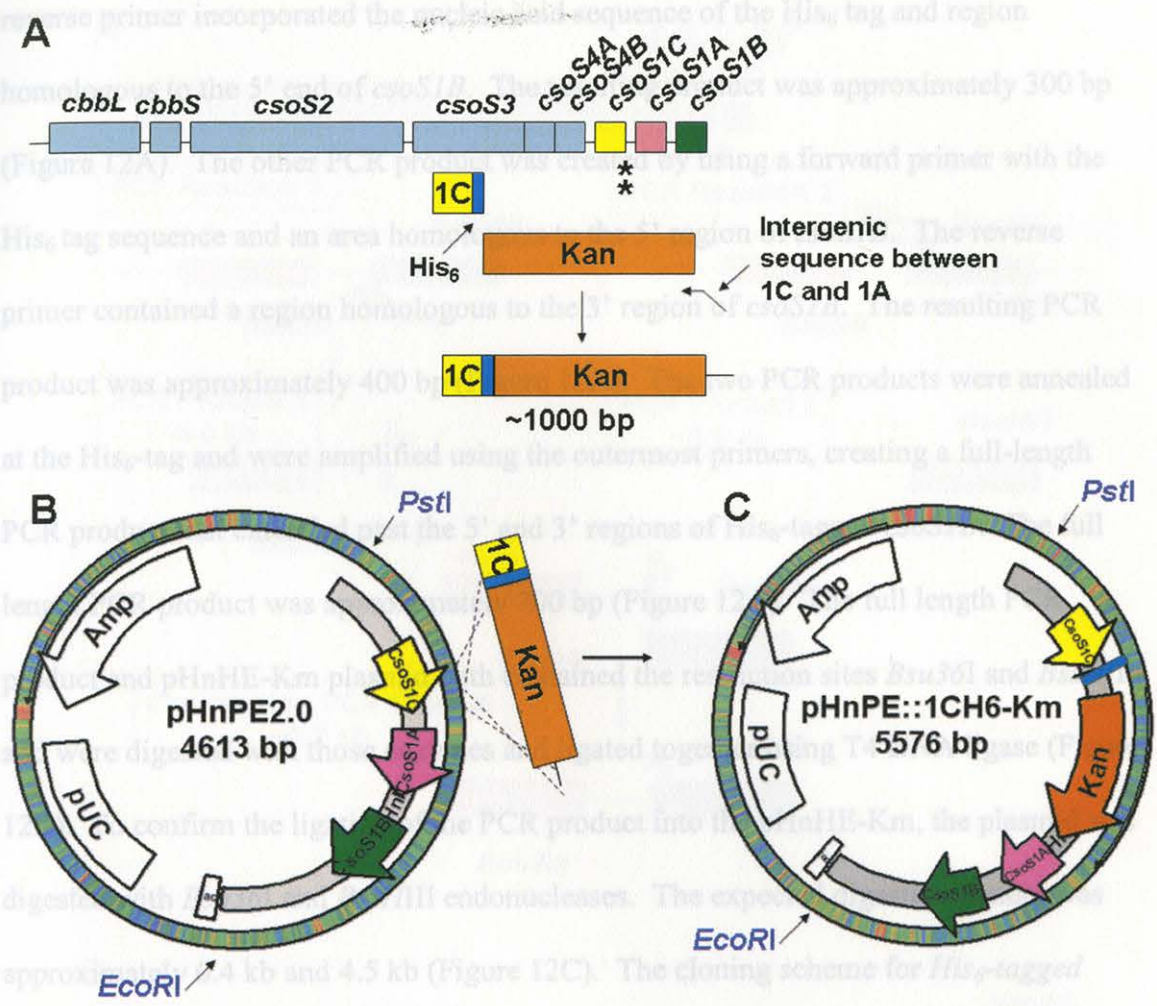

Figure 11. Strategy for Constructing pHnHE::1CH6-Km Plasmid. *(A)* PCR Amplification Strategy to generate the CsoS1C C-terminally His_6-tagged mutant. *(B)* pHnPE2.0 is a plasmid construct with the complete *csoS1C, csoS1A* and *csoS1B* genes within pUC18. *(C)* After recombination in *E. coli* DY330, the linear PCR fragments were incorporated into thepHnPE2.0 plasmid construct to create pHnHE::1CH6-Km plasmid construct. The asterisk represents the site in genome of *H. neapolitanus* in which the mutation will occur.

Generation of Plasmid Construct that Encodes N-terminally His_6-tagged CsoS1B

Overlap extension PCR was used to create an N-terminally *His_6-tagged csoS1B* plasmid construct (Figure 12A). Two PCR products were created by amplifying the regions upstream and downstream of the *csoS1B*. The upstream PCR product was created by using a forward primer that annealed to the 5' region of *csoS1A* and the

reverse primer incorporated the nucleic acid sequence of the His_6 tag and region homologous to the 5' end of *csoS1B*. The resulting product was approximately 300 bp (Figure 12A). The other PCR product was created by using a forward primer with the His_6 tag sequence and an area homologous to the 5' region of *csoS1B*. The reverse primer contained a region homologous to the 3' region of *csoS1B*. The resulting PCR product was approximately 400 bp (Figure 12A). The two PCR products were annealed at the His_6-tag and were amplified using the outermost primers, creating a full-length PCR product that extended past the 5' and 3' regions of His_6-tagged *csoS1B*. The full length PCR product was approximately 700 bp (Figure 12A). The full length PCR product and pHnHE-Km plasmid both contained the restriction sites *Bsu36*I and *BssH*II and were digested with those enzymes and ligated together using T4 DNA ligase (Figure 12B). To confirm the ligation of the PCR product into the pHnHE-Km, the plasmid was digested with *Bsu36*I and *BssH*III endonucleases. The expected digestion pattern was approximately 0.4 kb and 4.5 kb (Figure 12C). The cloning scheme for *His_6-tagged csoS1B* plasmid construct is outlined in Chapter IV. The sequence of the final plasmid construct was confirmed by the University of Maine DNA Sequencing Facility.

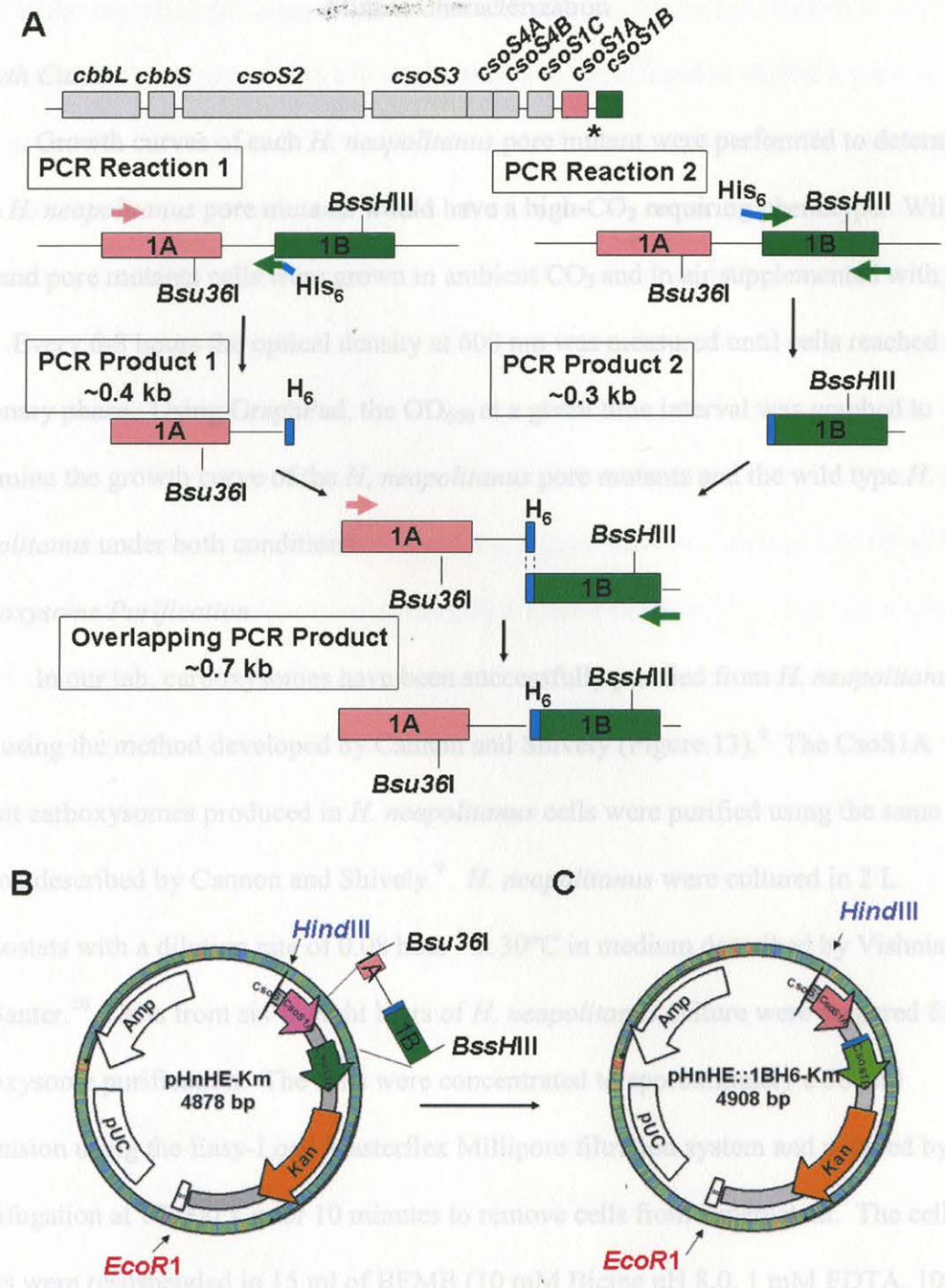

Figure 12. Strategy for Constructing pHnHE::1BH6-Km Plasmid. *(A)* PCR amplification strategy for the generation of a CsoS1B N-terminally His_6-tagged mutant. *(B)* pHnHE-Km is a plasmid construct which contains the *csoS1A and csoS1B* genes with a kanamycin cassette located on the 3' end of *csoS1B*. *(C)* The pHnHE-Km plasmid and linear PCR fragment were cut with *Bsu36*I and *Bss*HIII. The liner DNA fragment was ligated into pHnHE-Km. The asterisk represents the site in genome of *H. neapolitanus* in which the mutation will occur.

Mutant Characterization

Growth Curves

Growth curves of each *H. neapolitanus* pore mutant were performed to determine if the *H. neapolitanus* pore mutants would have a high-CO_2 requiring phenotype. Wild type and pore mutants cells were grown in ambient CO_2 and in air supplemented with 5% CO_2. Every 6-8 hours the optical density at 600 nm was measured until cells reached stationary phase. Using GraphPad, the OD_{600} at a given time interval was graphed to determine the growth curve of the *H. neapolitanus* pore mutants and the wild type *H. neapolitanus* under both conditions.

Carboxysome Purification

In our lab, carboxysomes have been successfully purified from *H. neapolitanus* cells using the method developed by Cannon and Shively (Figure 13).[9] The CsoS1A mutant carboxysomes produced in *H. neapolitanus* cells were purified using the same method described by Cannon and Shively.[9] *H. neapolitanus* were cultured in 2 L chemostats with a dilution rate of 0.08 $hour^{-1}$ at 30°C in medium described by Vishniac and Santer.[20] Cells from six to eight liters of *H. neapolitanus* culture were prepared for carboxysome purification. The cells were concentrated to approximately a 500 ml suspension using the Easy-Load Masterflex Millipore filtration system and pelleted by centrifugation at 12,000 x g for 10 minutes to remove cells from supernatant. The cell pellets were resuspended in 15 ml of BEMB (10 mM Bicine pH 8.0, 1 mM EDTA, 10 mM MgCl, and 20 mM $NaHCO_3$) buffer containing 1 mg/ml of lysozyme and 10 mM $MgSO_4$. The cell suspension were lysed with 15 ml of the detergent B-PER II and sonicated. To destroy genomic DNA, 150 µl of 1 mg/ml bovine pancreatic DNase I was

added to the sonicated cell suspension. The cell lysate was vigorously shaken at room temperature for 30 minutes. The cell suspension was centrifuged at 12,000 x g for 10 minutes and the supernatant was removed and centrifuged at 48,000 x g. The resulting pellet contained carboxysomes and cellular membranes. To remove some of the cellular membranes, the pellet was resuspended in 2 ml of BEMB and centrifuged at 1,000 x g for 4 minutes. The supernatant was loaded onto a 34 ml 10%-60% w/v continuous sucrose gradient in BEMB and centrifuged in a swinging bucket rotor at 104,000 x g for 35 minutes at 4°C. The carboxysomes appeared as a milky white band in the middle of the gradient. The carboxysomes were harvested and diluted in about 36 ml of BEMB and centrifuged using a fixed angle rotor at 150,000 x g for 2 hours at 4°C. The pellet was resuspended in ~1 ml of BEMB and stored at 4°C. The carboxysome suspension was analyzed using SDS-PAGE for the presence and stoichiometric ratios of carboxysome polypeptides.

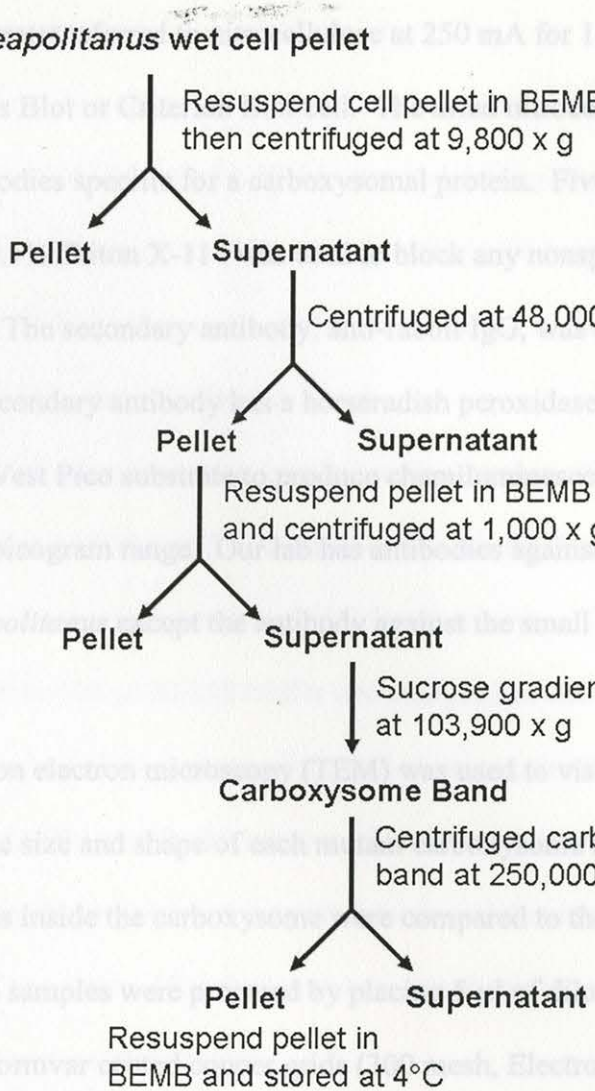

Figure 13. Flow Chart for the Preparation of Purified Carboxysomes from *H. neapolitanus*.

SDS-PAGE and Immunoblotting

Sodium dodecyl sulfate-polyacrylamide gel electrophoresis (SDS-PAGE) is a commonly used technique that separates polypeptides based on size; the polypeptides are visualized using Coomassie blue stain. SDS-PAGE was used to observe which carboxysomal polypeptides of the purified mutant carboxysomes. Immunoblotting was used to confirm the identity of each of the carboxysomal proteins except CsoS1A and CsoS1C because the antibody detected both proteins. Following SDS-PAGE, the

proteins were electrotransferred to nitrocellulose at 250 mA for 1 hour at 4°C using a BioRad Mini-Trans Blot or Criterion Blot cell. The dried nitrocellulose was incubated with primary antibodies specific for a carboxysomal protein. Five percent milk in 1X PBS pH 7.4 with 0.1% Triton X-114 was used to block any nonspecific binding sites on the nitrocellulose. The secondary antibody, anti-rabbit IgG, was used to bind the primary antibodies. The secondary antibody has a horseradish peroxidase attached that reacted with Supersignal West Pico substrate to produce chemiluminescent products that could be detected in the picogram range. Our lab has antibodies against all carboxysomal proteins of *H. neapolitanus* except the antibody against the small subunit of RubisCO.

TEM

Transmission electron microscopy (TEM) was used to visualize the purified carboxysomes. The size and shape of each mutant carboxysome and the amount of RubisCO molecules inside the carboxysome were compared to the wild type carboxysome. The samples were prepared by placing 5 µl of diluted mutant carboxysomes on formvar coated copper grids (300 mesh, Electron Microscopy Services) and incubating at room temperature for 30 seconds. The samples were stained with 5 µl of 1% w/v ammonium molybdate in BEMB pH 7.8 and air-dried for 30 seconds before visualizing on the Zeiss EM 109 or JEOL JEM-100 electron microscope. For the Zeiss EM 109, Kodak EM 4489 film were used to capture images and placed in D-19 developer solution for 4 minutes, rinsed with deionized water, incubated in fixer solution for 10 minutes, and rinsed with deionized water again for 20 minutes. Using the Epson Perfection V700 photo scanner, the air-dried developed film was scanned, and subsequently analyzed using Adobe Photoshop.

RubisCO Release Analysis

Using a 0.7 ml microfuge tube, purified carboxysomes with a total volume of 100 µl were centrifuged at 14,000 rpm for 30 minutes and the supernatant was carefully removed. The pellet was resuspended in exactly 100 µl. The supernatant and pellet were analyzed on SDS-PAGE for the presence of freed RubisCO in the supernatant.

Carboxysome Shell Disruption by Freeze-Break

Using a 0.7 ml microfuge tube, purified carboxysomes with a total volume of 100 µl were centrifuged at 14,000 rpm for 30 minutes and the supernatant was carefully removed and the pellet was incubated at -20°C for 45 minutes. The frozen pellet was rapidly resuspended in 100 µl BEMB buffer and analyzed or stored at 4°C until needed. To generate the enriched shell proteins of the carboxysome, the disrupted protein sample was centrifuged at 14,000 rpm for 30 minutes. The supernatant contained the free carboxysomal RubisCO particles and the pellet contained the shell proteins and the shell-associated RubisCO particles. The shell enriched sample and the freed RubisCO particles were analyzed on SDS-PAGE.

CHAPTER IV

RESULTS

Generation of CsoS1A Pore Mutants of *H. neapolitanus*

The following carboxysome pore mutants were generated by Dr. Balaraj B Menon. These CsoS1A pore mutants were generated to investigate the role of the CsoS1A hexamer pore in cellular growth, carboxysome composition, and function. The nucleotide sequence corresponding to the pore motif of the *csoS1A* gene was replaced with the nucleotide sequence that would lead to the conversion of G42 to L. Based on the predicted hexamer structures (models from Dr. Fei Cai and Seth Axen), the mutation at the 42nd position of CsoS1A will narrow the pore opening (Figure 14). The *csoS1A* gene contains two restriction sites, *Pml*I and *Bsu*36I, which are located upstream and downstream, respectively, of the desired mutation. Two PCR products were amplified for overlap extension PCR. One of the PCR products contained the desired mutation and the 5' region of the gene, including the *Pml*I restriction site (Figure 15). The other PCR product included the mutation and the 3' region of the gene, which including the *Bsu*36I restriction site. The two PCR products were annealed across the mutated site and extended using the outermost 3' and 5' primers, thereby generating the full-length amplicon (Figure 15). The newly synthesized PCR product was digested with *Pml*I and *Bsu*36I and used to replace the corresponding region of the pHnHE::G43A plasmid construct which has an alanine (A) codon at the 43rd position in the *csoS1A* gene instead of a glycine codon and a kanamycin cassette needed for transformant selection (Figure 12).[45] The resulting plasmids containing the G42L and the F40D mutations in the *csoS1A*

gene were named pHnHE::G42L and pHnHE::F40D, respectively (Figure 16). *H. neapolitanus* was transformed with the plasmid constructs by electroporation.

Figure 14. Pore Cross Sections of the Predicted Structure and Charge of the Pore of the CsoS1A Hexamer with each Amino Acid Alteration. The red color indicates a negative surface charge and blue represents a positive surface charge.

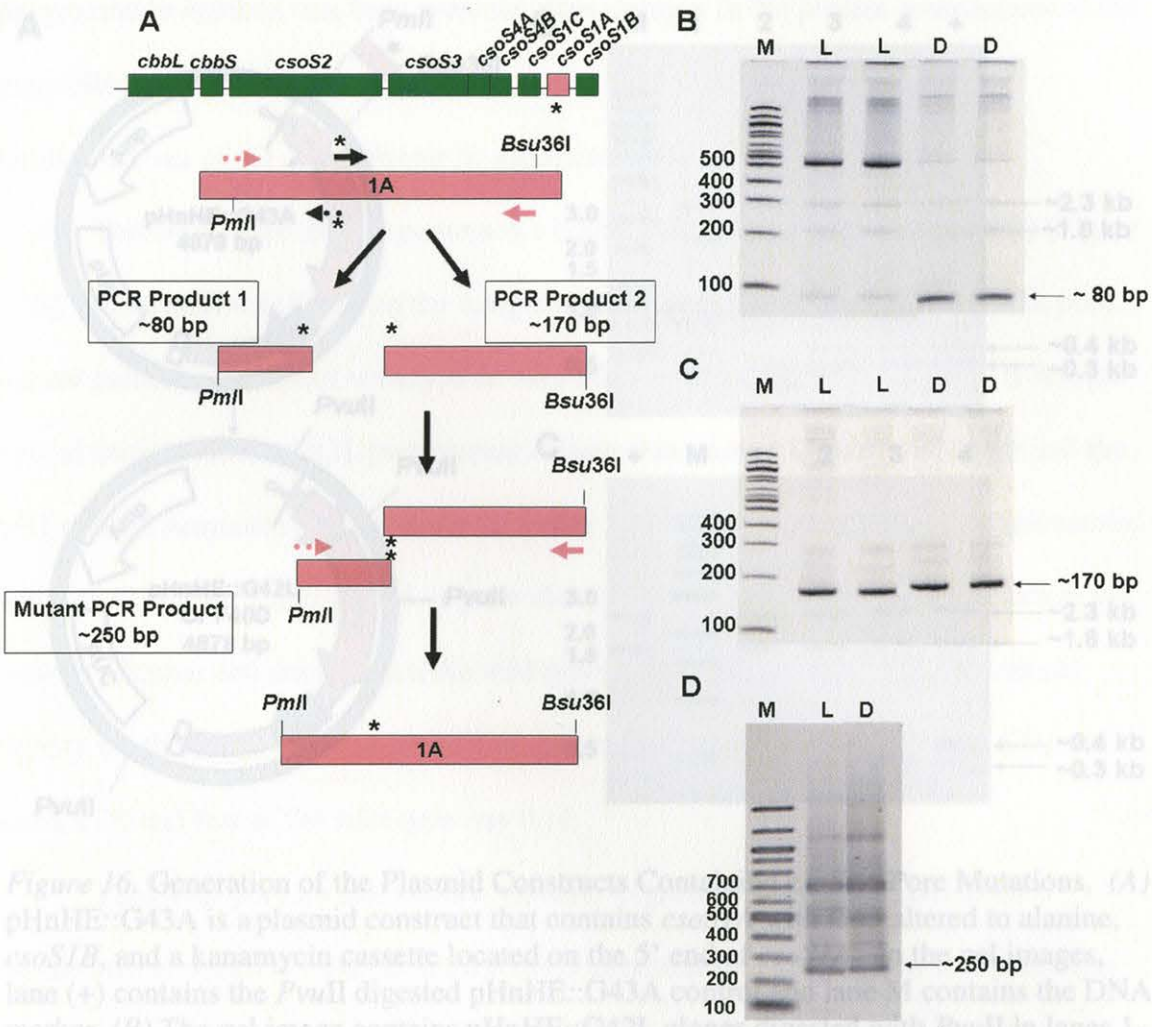

Figure 15. Strategy for Site-Directed Mutagenesis to Construct Pore Mutation Plasmids. *(A)* The site-directed mutagenesis strategy for pore mutation plasmid constructs which involved amplifying *csoS1A* using primers containing the desired pore mutation. *(B)* The gel images are labeled, L for G42L, D for F40D, and M for protein marker. The 6% polyacrylamide gel contains the 80 bp PCR products 1 of 5' region of *csoS1A* containing the restriction site, *Pml*I, for each pore mutation. The band at 500 bp may be due to nonspecific interactions of the primers with the DNA template *(C)* The 6% polyacrylamide gel contains the 170 bp PCR products 2 of 3' region of *csoS1A* containing the restriction site, *Bsu*36I, for each pore mutation. *(D)* The 1% agarose gel contains the full length 250 bp mutant PCR product of *csoS1A* that contains both restriction sites, *Pml*I and *Bsu*36I, for each pore mutation. The additional bands may be due to the amplification of the nonspecific PCR products in image *(B)*. The asterisk represents the mutation site.

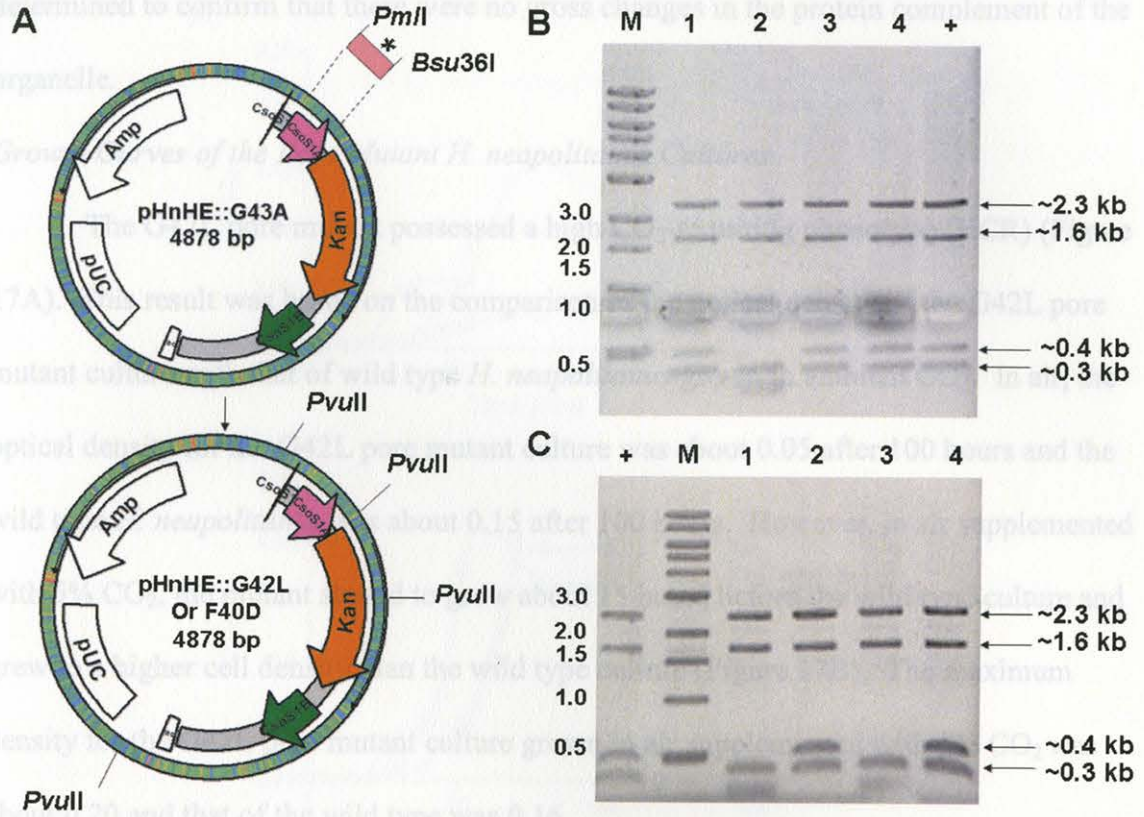

Figure 16. Generation of the Plasmid Constructs Containing *csoS1A* Pore Mutations. *(A)* pHnHE::G43A is a plasmid construct that contains *csoS1A* with G43 altered to alanine, *csoS1B*, and a kanamycin cassette located on the 5' end of *csoS1A*. In the gel images, lane (+) contains the *Pvu*II digested pHnHE::G43A control and lane M contains the DNA marker. *(B)* The gel image contains pHnHE::G42L clones digested with *Pvu*II in lanes 1-4. Only clones in lanes 1, 3, and 4 of G42L had the insert. *(C)* Lanes 1-4 contains pHnHE::F40D clones digested with *Pvu*II. Only the F40D clones in lanes 2 and 4 had the insert.

Pore Mutant Characterization

It has been shown that when a carboxysome-containing organism has been mutated, which results in a nonfunctional carboxysome, the organism requires additional CO_2 to grow efficiently.[10,53-56] Therefore, growth curves of the pore mutants and wild type *H. neapolitanus* cultures were performed in air, and in air supplemented with 5% CO_2. These growth conditions tested if the altered pore properties would affect the growth of the *H. neapolitanus* cultures. The composition of the carboxysomes was

determined to confirm that there were no gross changes in the protein complement of the organelle.

Growth Curves of the Pore Mutant H. neapolitanus Cultures

The G42L pore mutant possessed a high CO_2-requiring phenotype (HCR) (Figure 17A). This result was based on the comparison of the optical density of the G42L pore mutant culture with that of wild type *H. neapolitanus* grown in ambient CO_2. In air, the optical density for the G42L pore mutant culture was about 0.05 after 100 hours and the wild type *H. neapolitanus* was about 0.15 after 100 hours. However, in air supplemented with 5% CO_2, the mutant started to grow about 15 hours before the wild type culture and grew to a higher cell density than the wild type culture (Figure 17B). The maximum density for the G42L pore mutant culture grown in air supplemented with 5% CO_2 was about 0.20 and that of the wild type was 0.16.

The F40D pore mutant culture was able to grow in ambient air and in air supplemented with 5% CO_2. In air, the F40D pore mutant cultures grew to a maximum optical density of 0.1(Figure 17A). In air supplemented with 5% CO_2, the F40D pore mutant and wild type *H. neapolitanus* cultures grew to the same maximum optical density (Figure 17B). However, the F40D pore mutant culture exhibited biphasic growth in both air and air supplemented with 5% CO_2. The F40D pore mutant cultures began to grow at approximately 25 hours and after 5 hours the growth rate leveled off, then the growth resumed after approximately 25 hours (Figure 17).

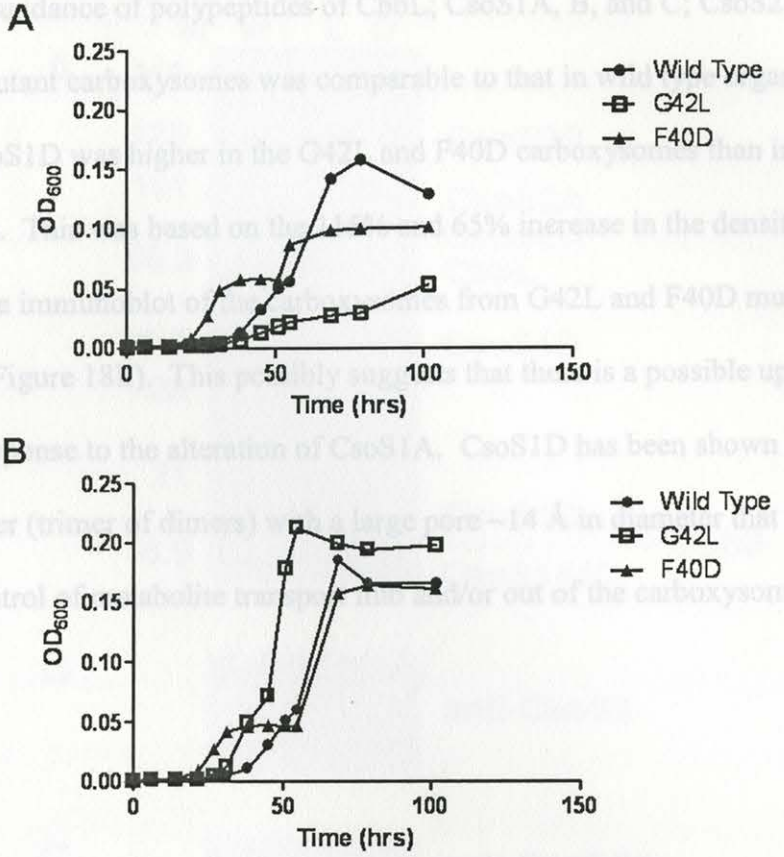

Figure 17. Representative Growth Curves of *H. neapolitanus* CsoS1A Pore Mutants. *(A)* Batch cultures of wild type and pore mutant were grown in air at 30°C. The G42L pore mutant grew at a slower rate and the F40D pore mutant had a biphasic growth pattern when compared to the wild type culture. *(B)* Wild type and pore mutant *H. neapolitanus* cultures were grown in air supplemented with 5% CO_2 at 30°C. The G42L pore mutant grew to a higher density and F40D pore mutant had a biphasic growth pattern.

Polypeptide Composition of the Purified Pore Mutant Carboxysomes

SDS-PAGE and immunoblotting were used to determine the relative polypeptide composition of the pore mutant and wild type carboxysomes (Figure 18). Antibodies against the large subunit of RubisCO (CbbL), the major shell proteins (CsoS1A, B, and C), the largest shell components (CsoS2A and B), the carbonic anhydrase (CsoSCA), and CsoS1D were used detect the presence and establish the relative abundance of the carboxysomal polypeptides.

The abundance of polypeptides of CbbL; CsoS1A, B, and C; CsoS2A and B; and CsoSCA in mutant carboxysomes was comparable to that in wild type organelles. The amount of CsoS1D was higher in the G42L and F40D carboxysomes than in wild type carboxysomes. This was based on the 115% and 65% increase in the density of the CsoS1D on the immunoblot of the carboxysomes from G42L and F40D mutants, respectively (Figure 18E). This possibly suggests that there is a possible up-regulation of CsoS1D in response to the alteration of CsoS1A. CsoS1D has been shown to form a pseudohexamer (trimer of dimers) with a large pore ~14 Å in diameter that may play a role in the control of metabolite transport into and/or out of the carboxysome.[44]

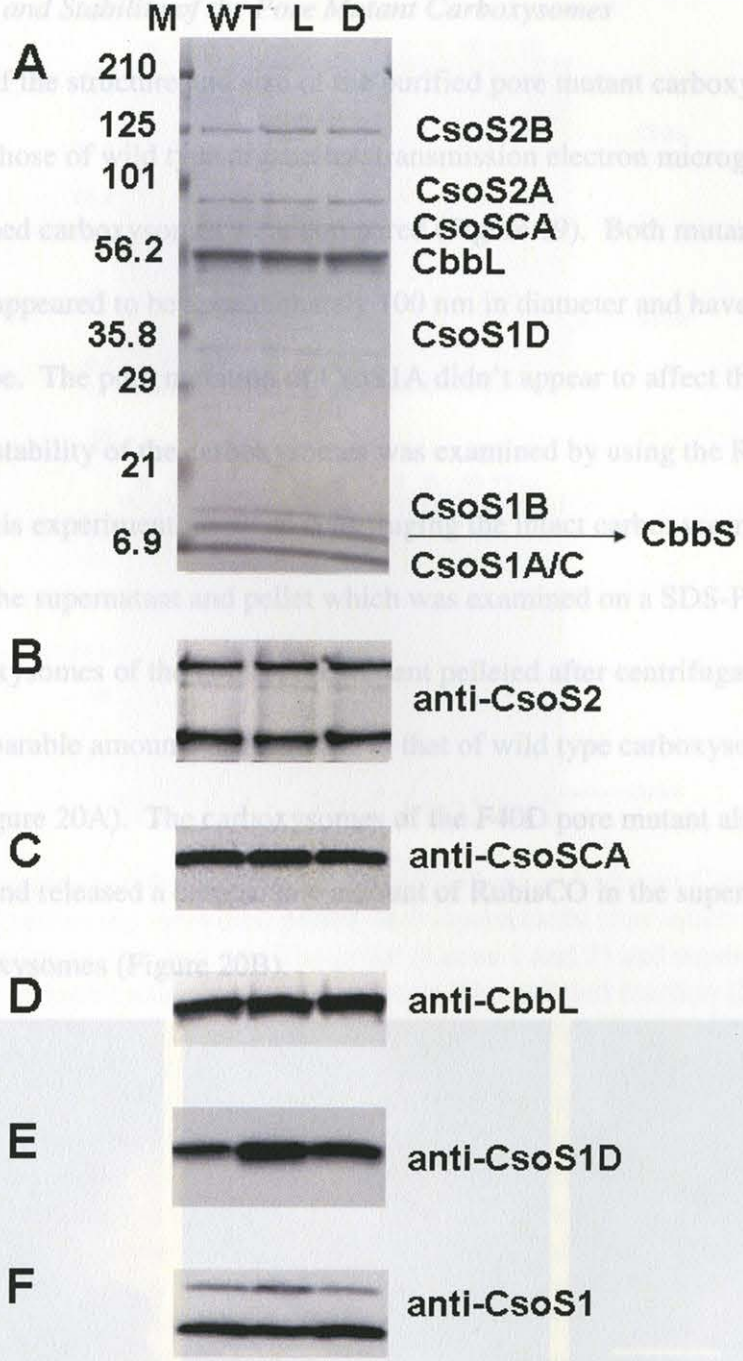

Figure 18. Analysis of the Polypeptide Composition of Purified Carboxysomes. *(A)* The SDS-PAGE shows the polypeptides of the purified wild type and pore mutant carboxysomes. M = molecular weight standards, L = G42L, and D = F40D carboxysomes. The polypeptides were electrotransferred onto nitrocellulose paper and developed with the respective antibodies (Panels B through F).

Structure, Size, and Stability of the Pore Mutant Carboxysomes

To test if the structure and size of the purified pore mutant carboxysomes were comparable to those of wild type organelles, transmission electron micrographs of negatively stained carboxysomes were compared (Figure 19). Both mutant and wild type carboxysomes appeared to be approximately 100 nm in diameter and have a similar polyhedral shape. The pore mutation of CsoS1A didn't appear to affect the overall structure. The stability of the carboxysomes was examined by using the RubisCO release experiment. This experiment involved centrifuging the intact carboxysome pore mutants and collecting the supernatant and pellet which was examined on a SDS-PAGE (Figure 20). The carboxysomes of the G42L pore mutant pelleted after centrifugation and released a comparable amounts of RubisCO to that of wild type carboxysomes in the supernatant (Figure 20A). The carboxysomes of the F40D pore mutant also pelleted after centrifugation and released a comparable amount of RubisCO in the supernatant to that of wild type carboxysomes (Figure 20B).

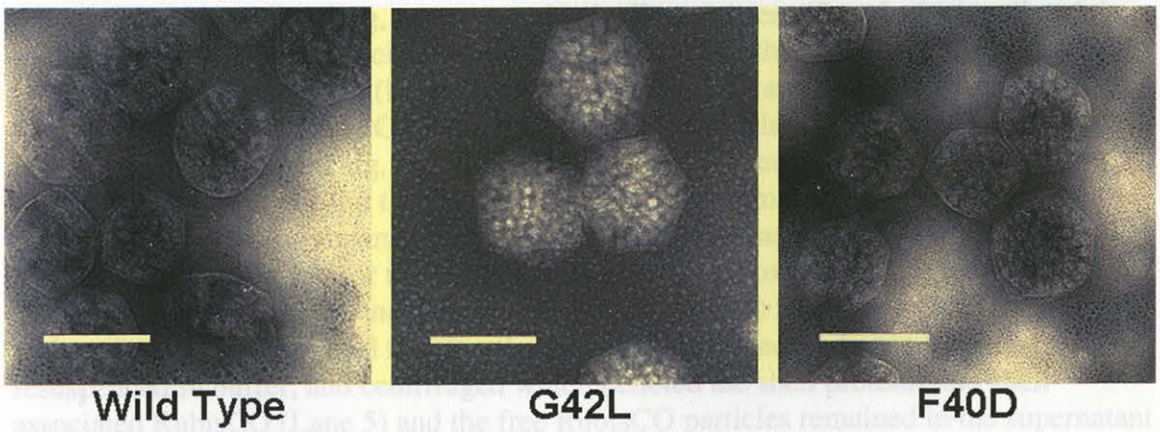

Figure 19. Transmission Electron Micrographs of Purified Carboxysomes. Purified *H. neapolitanus* carboxysomes were stained with 1% ammonium molybdate and observed under a transmission electron microscope at 30,000 fold magnification. The scale bars represent 100 nm. The overall size and shape of the pore mutant carboxysomes are comparable to those of wild type organelles.

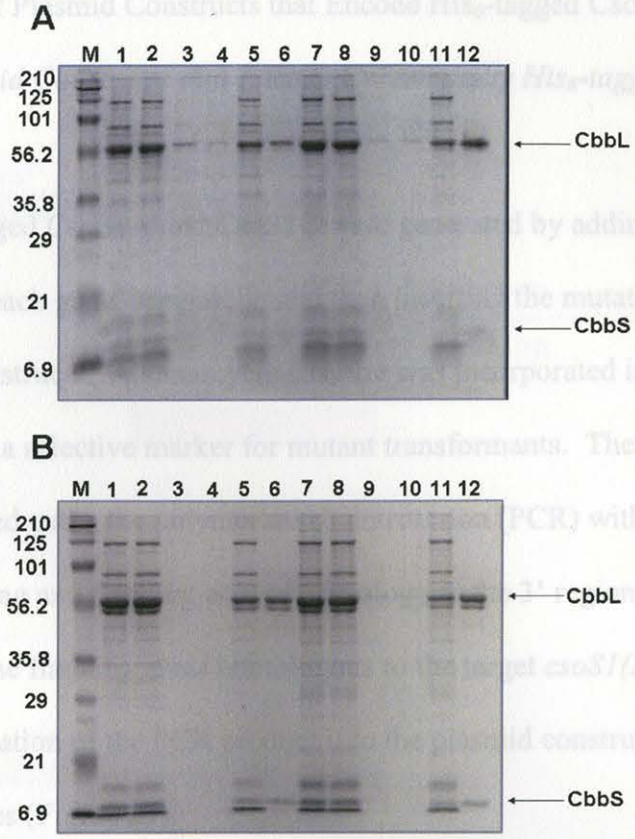

Figure 20. Comparison of the Stability of the Wild Type and Mutant Carboxysomes. The SDS-PAGE gel shows the recovered pellets and supernatants after intact or freeze-broken carboxysomes were centrifuged. *(A)* The pellet (Lanes 1 and 2) and supernatant (Lanes 3 and 4) fractions of intact wild type carboxysomes. The pelleted fraction (Lane 2) was disrupted by freeze-breaking, resuspended in buffer, and centrifuged which pelleted the shell proteins and shell-associated RubisCO (Lane 5) and the free RubisCO particles remained in the supernatant (Lane 6). The pellet (Lanes 7 and 8) and supernatant (Lanes 9 and 10) fractions of intact G42L carboxysomes. The pelleted fraction (Lane 8) was disrupted by freeze-breaking, resuspended in buffer, and centrifuged which pelleted the shell proteins (Lane 11) and the free RubisCO particles remained in the supernatant (Lane 12). There is a comparable amount of RubisCO released into the supernatant fractions (Lanes 3 and 9) for the wild type and G42L carboxysomes, respectively. *(B)* The pellet (Lanes 1 and 2) and supernatant (Lanes 3 and 4) fractions of intact wild type carboxysomes. The pelleted fraction (Lane 2) was disrupted by freeze-breaking, resuspended in buffer, and centrifuged which pelleted the shell proteins and shell-associated RubisCO (Lane 5) and the free RubisCO particles remained in the supernatant (Lane 6). The pellet (Lanes 7 and 8) and supernatant (Lanes 9 and 10) fractions of intact F40D carboxysomes. There is a comparable amount of RubisCO released into the supernatant fractions (Lanes 3 and 9) for the wild type and F40D carboxysomes, respectively. The pelleted fraction (Lane 8) was disrupted by freeze-breaking, resuspended in buffer, and centrifuged which pelleted the shell proteins (Lane 11) and the free RubisCO particles remained in the supernatant (Lane 12).

Generation of Plasmid Constructs that Encode His_6-tagged CsoS1 Paralogs

Generation of Plasmid Constructs that Encode C-Terminally His_6-tagged CsoS1A and CsoS1C

The His_6-tagged CsoS1A and CsoS1C were generated by adding six histidine codons on the 3' of each gene, separately, and then inserting the mutated genes into separate plasmid constructs. A kanamycin cassette was incorporated into each plasmid construct to serve as a selective marker for mutant transformants. The kanamycin cassette was amplified using the polymerase chain reaction (PCR) with primers containing the His_6-tag and flanking area of homology to the 3' region of *csoS1(A or C)* gene (Figure 21). The flanking areas homologous to the target *csoS1(A or C)* were needed for recombination of the PCR product into the plasmid construct containing the wild type *csoS1* genes (Figure 21).

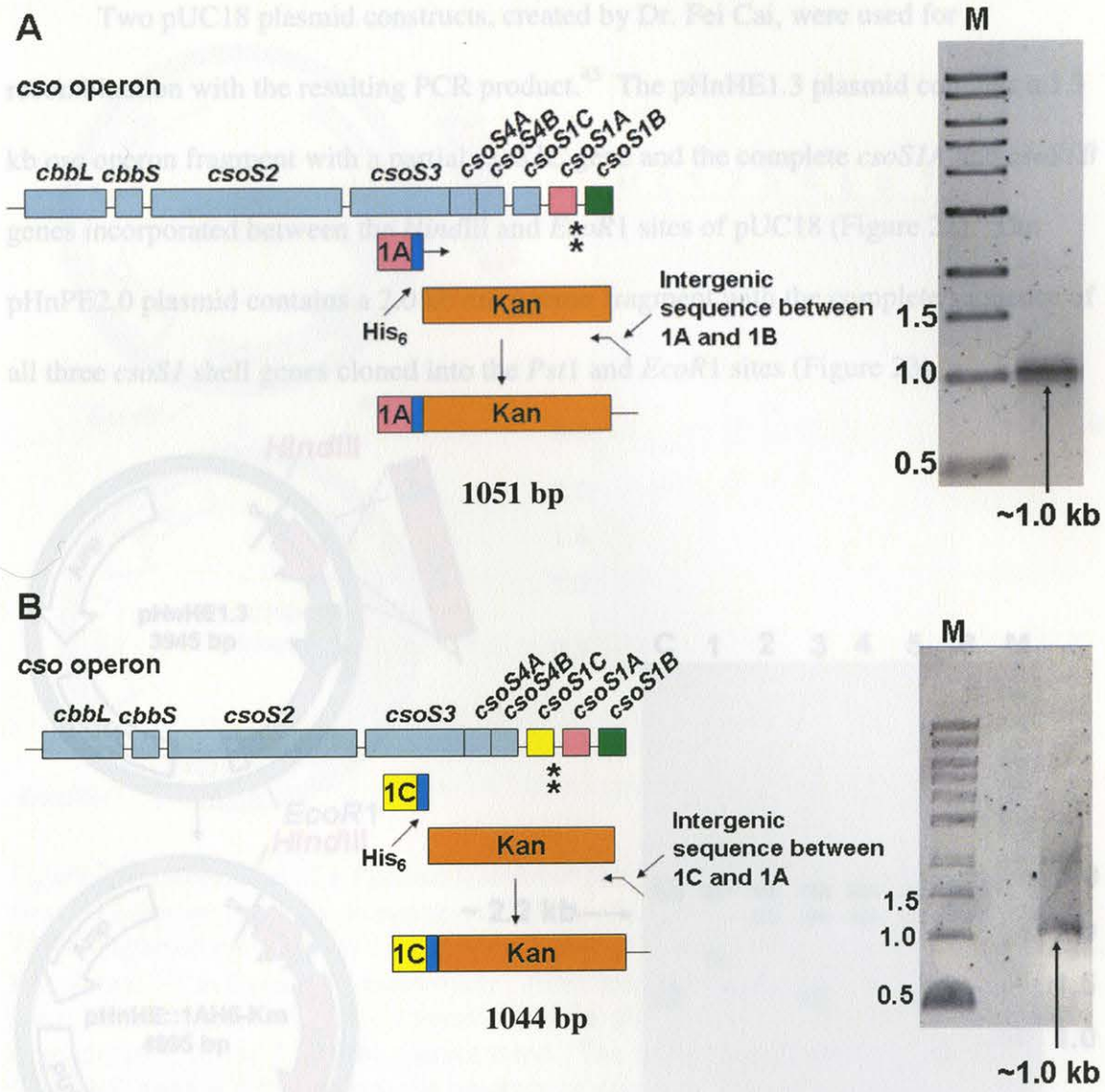

Figure 21. PCR Amplification Strategy to Generate the CsoS1A and CsoS1C C-Terminally His_6-tagged Mutant. *(A)* PCR amplification strategy for the generation of a CsoS1A C-terminally His_6-tagged mutant is illustrated; to the right is the image of a 0.8% agarose gel which shows the resulting PCR product with the expected molecular weight of ~1000 bp. The asterisks represent the insertion sites of the PCR amplified kanamycin cassette with the primers containing the six histidine codons and homologous regions to *csoS1A* and *csoS1B* genes in the *cso* operon. *(B)* PCR Amplification Strategy to generate the CsoS1C C-terminally His_6-tagged mutant is illustrated; to the right is the 0.8% agarose gel image with the resulting PCR product with the expected molecular weight of ~1000 bp. The asterisk represents the mutation site.

Two pUC18 plasmid constructs, created by Dr. Fei Cai, were used for recombination with the resulting PCR product.[45] The pHnHE1.3 plasmid contains a 1.3 kb *cso* operon fragment with a partial *csoS1C* gene and the complete *csoS1A* and *csoS1B* genes incorporated between the *Hind*lll and *EcoR*1 sites of pUC18 (Figure 22). The pHnPE2.0 plasmid contains a 2.0 kb *cso* operon fragment with the complete sequence of all three *csoS1* shell genes cloned into the *Pst*1 and *EcoR*1 sites (Figure 23).

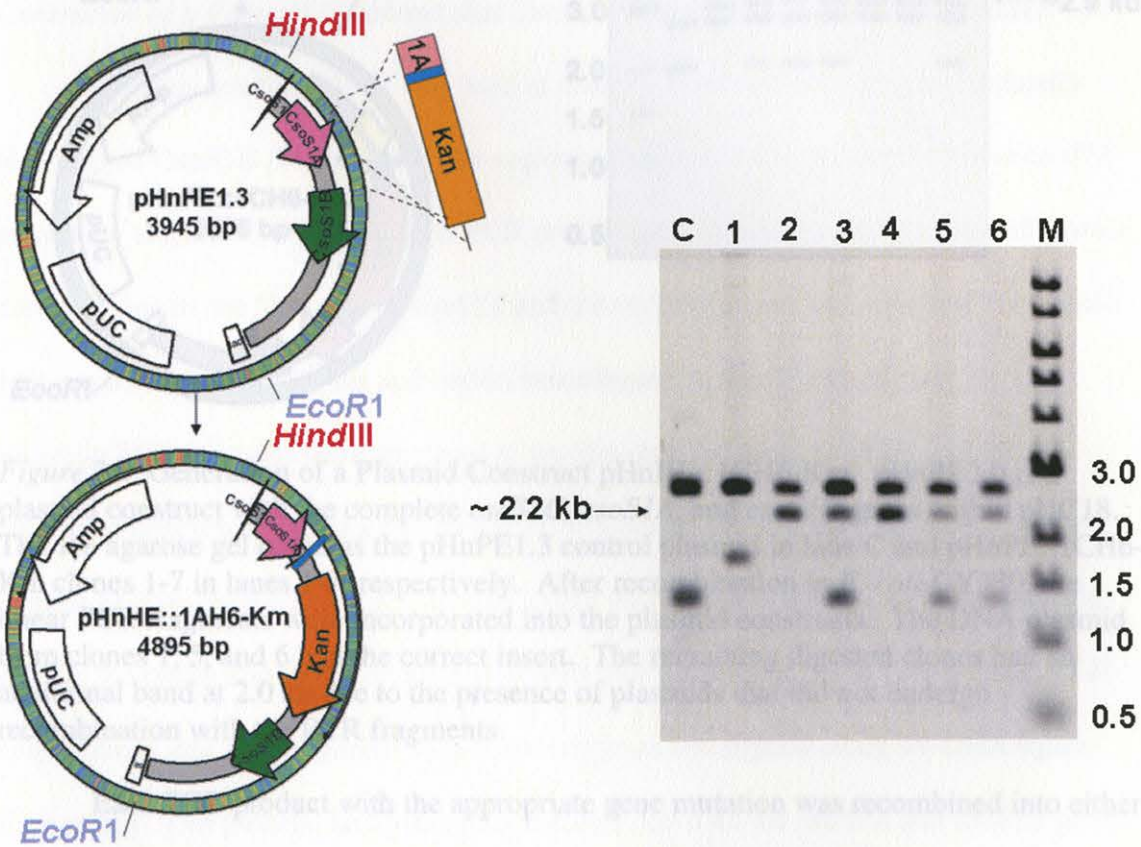

Figure 22. Generation of a Plasmid Construct pHnHE::1AH6-Km. pHnHE1.3 is a plasmid construct with a partial *csoS1C* and complete *csoS1A* and *csoS1B* genes within pUC18. The 1% agarose gel contains the pHnHE1.3 control plasmid in lane C and pHnHE::1AH6-Km clones 1-6 in lanes 1-6, respectively. After recombination in *E. coli* DY330, the linear PCR fragments were incorporated into the plasmid constructs. The DNA plasmid from clones 2 and 4 had the correct insert. The remaining digested clones had an additional band at 1.3 kb due to the presence of plasmids that did not undergo recombination with the linear PCR fragments.

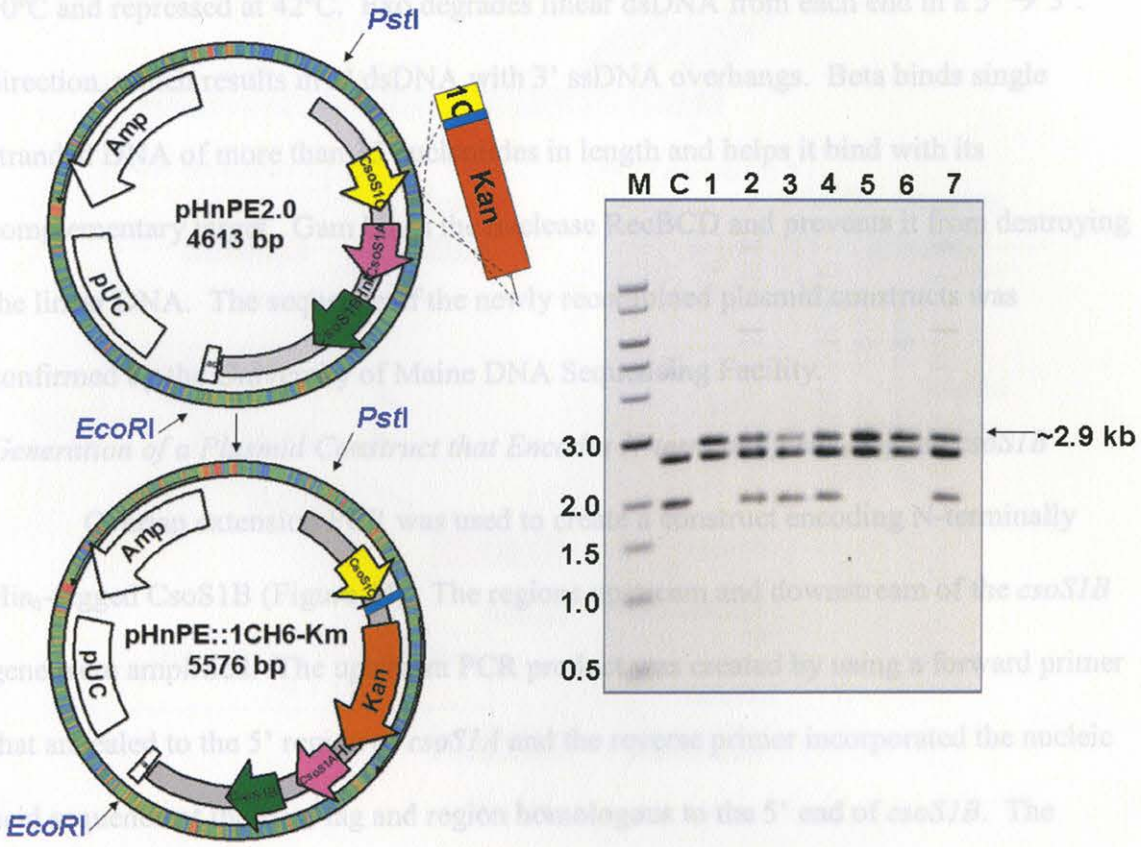

Figure 23. Generation of a Plasmid Construct pHnHE::1CH6-Km. pHnPE2.0 is a plasmid construct with the complete *csoS1C, csoS1A,* and *csoS1B* genes within pUC18. The 1% agarose gel contains the pHnPE1.3 control plasmid in lane C and pHnPE::1CH6-Km clones 1-7 in lanes 1-7, respectively. After recombination in *E. coli* DY330, the linear PCR fragments were incorporated into the plasmid constructs. The DNA plasmid from clones 1, 5, and 6 had the correct insert. The remaining digested clones had an additional band at 2.0 kb due to the presence of plasmids that did not undergo recombination with the PCR fragments.

Each PCR product with the appropriate gene mutation was recombined into either pHnHE1.3 or pHnPE2.0 in the DY330 strain of *Escherichia coli*. The recombination system of DY330 requires less than 100 bp of homology in linear DNA for recombination to occur with a target gene in a circular plasmid. The genes *exo, bet,* and *gam* of the defective λ prophage that encode the proteins Exo, Beta, and Gam, respectively, were inserted into the genome of *E. coli* DY330. The λ prophage is controlled by a temperature-sensitive λ cI-repressor.[57] The cI-repressor is induced at

30°C and repressed at 42°C. Exo degrades linear dsDNA from each end in a 5' → 3' direction, which results in 3' dsDNA with 3' ssDNA overhangs. Beta binds single stranded DNA of more than 35 nucleotides in length and helps it bind with its complementary target. Gam binds the nuclease RecBCD and prevents it from destroying the linear DNA. The sequence of the newly recombined plasmid constructs was confirmed by the University of Maine DNA Sequencing Facility.

Generation of a Plasmid Construct that Encodes N-terminally His_6-tagged csoS1B

Overlap extension PCR was used to create a construct encoding N-terminally His_6-tagged CsoS1B (Figure 24). The regions upstream and downstream of the *csoS1B* gene were amplified. The upstream PCR product was created by using a forward primer that annealed to the 5' region of *csoS1A* and the reverse primer incorporated the nucleic acid sequence of the His_6-tag and region homologous to the 5' end of *csoS1B*. The resulting PCR products were annealed at the His_6-tag and were amplified using the outermost primers, creating a full-length PCR product that extended past the 5' and 3' regions of His_6-tagged *csoS1B*. The full length PCR product and pHnHE-Km plasmid contain the restriction sites *Bsu36*I and *BssH*II that are present in the *csoS1A* gene of *H. neapolitanus* and were digested with those enzymes and ligated using T4 DNA ligase (Figure 25). The pHnHE-Km plasmid construct contained the *csoS1A* and *csoS1B* genes with a kanamycin cassette located downstream of *csoS1B*. The sequence of the final plasmid construct was confirmed by the University of Maine DNA Sequencing Facility.

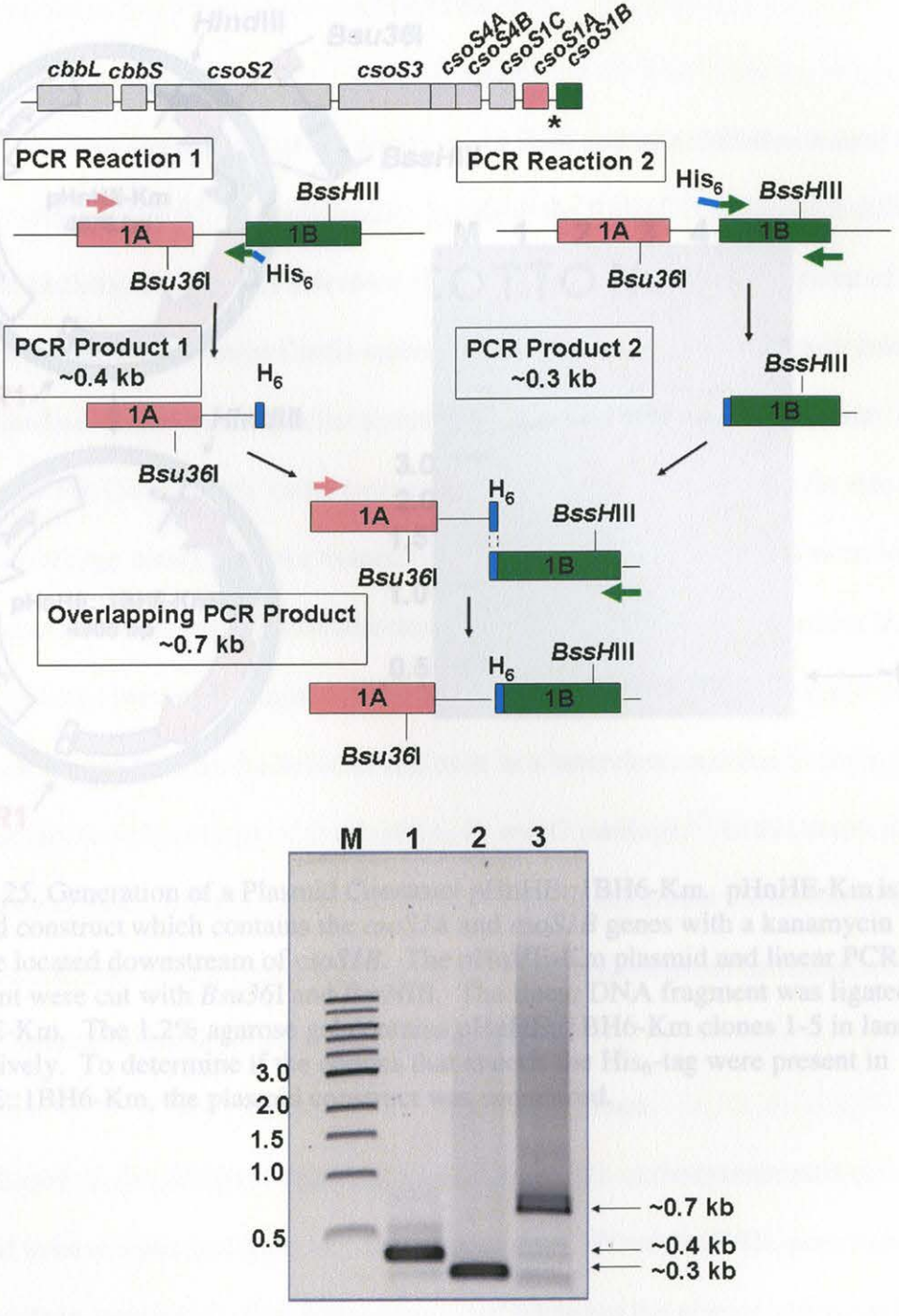

Figure 24. PCR Amplification Strategy to Generate *csoS1B* encoding an N-Terminally His_6-tagged Protein. PCR amplification strategy for the generation of a CsoS1B N-terminally His_6-tagged mutant is illustrated; below is a 1.2% agarose gel, which contains DNA Marker in lane M, PCR product 1 in lane 1, PCR product 2 in lane 2, and the overlapping PCR product in lane 3. The asterisk represents the mutation site.

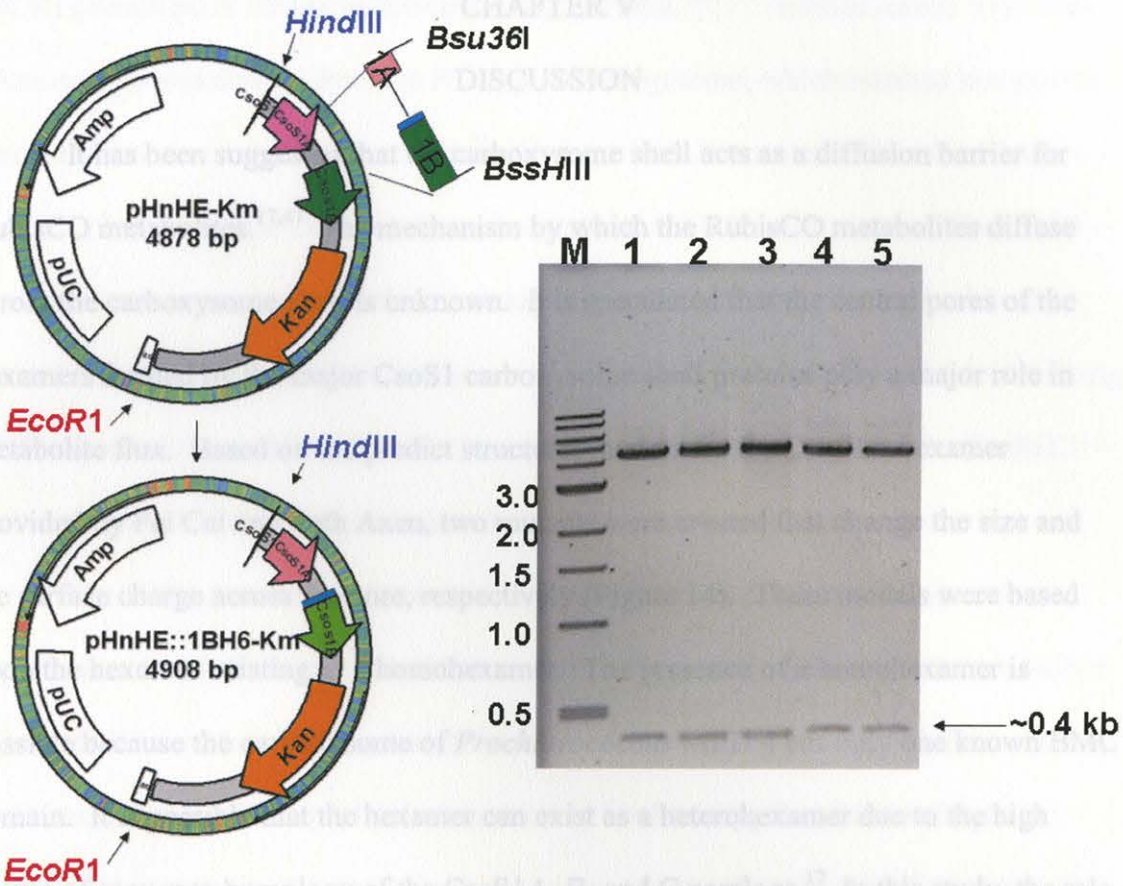

Figure 25. Generation of a Plasmid Construct pHnHE::1BH6-Km. pHnHE-Km is a plasmid construct which contains the *csoS1A* and *csoS1B* genes with a kanamycin cassette located downstream of *csoS1B*. The pHnHE-Km plasmid and linear PCR fragment were cut with *Bsu36*I and *BssH*III. The linear DNA fragment was ligated into pHnHE-Km. The 1.2% agarose gel contains pHnHE::1BH6-Km clones 1-5 in lanes 1-5, respectively. To determine if the codons that encode the His_6-tag were present in pHnHE::1BH6-Km, the plasmid construct was sequenced.

CHAPTER V

DISCUSSION

It has been suggested that the carboxysome shell acts as a diffusion barrier for RubisCO metabolites.[17,47] The mechanism by which the RubisCO metabolites diffuse across the carboxysome shell is unknown. It is speculated that the central pores of the hexamers formed by the major CsoS1 carboxysome shell proteins play a major role in metabolite flux. Based on the predict structural models for the CsoS1A hexamer provided by Fei Cai and Seth Axen, two mutants were created that change the size and the surface charge across the pore, respectively (Figure 14). These models were based upon the hexamer existing as a homohexamer. The presence of a homohexamer is possible because the carboxysome of *Prochlorococcus* MED 4 has only one known BMC domain. It is possible that the hexamer can exist as a heterohexamer due to the high degree of sequence homology of the CsoS1A, B, and C paralogs.[17] In this study, the role of the hexamer pore in the diffusion of RubisCO metabolites across the carboxysome shell was examined by the changes in growth and the composition of carboxysomes from the pore mutants of *Halothiobacillus neapolitanus*.

Growth of the G42L Pore Mutant

Based on the predicted structural models, the G42L carboxysome pore mutant appeared to have a plugged pore for CsoS1A hexamers. Since the G42L pore mutant grew poorly in ambient air, this data suggests that replacing the glycine residue at the 42nd position of the CsoS1A polypeptide with a leucine may produce a carboxysome that, potentially, is not fully functional. Previous studies have shown that creating mutations resulting in carboxysomes that are not fully functional results in a high CO_2-requiring

(HCR) phenotype in carboxysome-containing bacteria.[10,53-56] Similar results were seen when *csoS1A* was deleted from the *H. neapolitanus* genome, which resulted in a mutant that grew at a slow rate in ambient air.[58] It has not been determined if the CsoS1A protein is being incorporated into the carboxysomes of G42L pore mutant. The CsoS1 antibodies can interact with all three paralogs of CsoS1. If homohexamers are being formed then the presence of six leucines or six aspartates in the pore may be destabilizing the hexamer. This could result in the incorporation of higher amounts of the CsoS1C hexamer instead of the CsoS1A hexamer into the carboxysome shell.

The G42L pore mutant grew to a higher optical density than wild type in air supplemented with 5% CO_2. Possible issues with the growth curves were the production of extracellular sulfur particles, metabolic intermediates in the sulfur catabolism pathway of *H. neapolitanus*. The spectrophotometer may be detecting the additional light scattering that is due to the insoluble sulfur and not due to the presence of the cells. The increased production of insoluble sulfur may indicate that the mutant cells do not oxidize thiosulfate as efficiently as wild type cells. There has been research that examined the correlation between sulfur oxidation and the assimilation of carbon due to the needed energy and reducing equivalents from the sulfur metabolic pathway in the carbon assimilation pathway.[59] When excess thiosulfate was present, insoluble intermediates of the sulfur oxidation pathway were produced that remained in the media until the cells utilized it as an energy source.[59] G42L cells may not be utilizing the thiosulfate as rapidly as wild type cells and there is an accumulation of sulfur intermediates that are precipitating in the media. If not enough energy is being produced from the sulfur oxidation pathway then the Calvin-Benson-Bassham cycle will not be able to regenerate

the CO_2 acceptor RuBP and carbon dioxide fixation will be prevented. Another reason the optical density was higher for G42L pore mutant cells in air supplemented with 5% CO_2 could be due to the presence of Form II RubisCO. *H. neapolitanus* has two types of RubisCO, Form 1 and Form II. Form I RubisCO is sequestered into the carboxysome and Form II remains in the cytosol.[25] Based on studies conducted by Yoshizawa et al., the Proteobacteria *Hydrogenovibrio marinus* when grown in air supplemented with 2% CO_2 expressed Form II RubisCO and Form I RubisCO, and when grown at a lower level of CO_2 the organism expressed predominately Form I RubisCO.[60]

Growth of the F40D Pore Mutant

The pore mutant in which an aspartate replaced a phenylalanine in the conserved pore motif of CsoS1A, F40D, grew to a lower cellular density than wild type *H. neapolitanus* and possessed a biphasic growth pattern in air and air supplemented with 5% CO_2. A possible explanation for the biphasic growth could be the utilization of reduced sulfur compounds as an energy source. F40D pore mutants may be able to utilize the thiosulfate in the media more rapidly than wild type initially, but there could be a transition phase inside the cell in which thiosulfate has been completely utilized and other sulfur intermediates in the environment must be transported into the cell to be metabolized as an energy source. This is illustrated in Figure 1 step *(h)* in which the thiosulfate in the media is reduced to elemental sulfur. In order for sulfur to be transported into the cell, it must be converted to sulfide and using membrane sulfide transporters, the sulfide is transported into the cell (Figure 1*(i)*). If there is not enough energy being produced by the sulfur oxidation pathway then the Calvin-Benson-Bassham cycle cannot regenerate the CO_2 acceptor RuBP, which will prevent CO_2 fixation.

Another explanation for the biphasic growth could also be caused by changes in metabolite flux into and out of the carboxysomes. The change in the charge on the pore may not be enough to affect diffusion of the RubisCO metabolites across the carboxysome shell. The growth rate of the F40D pore mutant could be leveling off after just 25 hours due to low amounts of the product of RubisCO, 3-PGA, being released into the cytosol. There could be a build up of the negatively charged 3-PGA in the carboxysome, but due to the change in the surface charge on the pore, the diffusion of the 3-PGA out of the carboxysome could be limited. This could be causing negative feedback inhibition of RubisCO due to the product remaining in the active site which could be preventing the substrates from entering the active site of RubisCO. The 3-PGA molecules are the carbon skeletons needed to regenerate the CO_2 acceptor RuBP, and the reduction of RuBP will limit carbon dioxide fixation and the cultures will not be able to grow efficiently.

Based on the growth characteristics of the F40D pore mutant it is possible that the mutation to CsoS1A protein does affect the overall growth. This coincides with previous studies that predicted that the charge of the pore could play a role in attracting negatively charged metabolites, bicarbonate, RuBP, and 3-PGA.[17] Tsai et al. proposed that there are electrostatic interactions between the RubisCO metabolites and the residues of the CsoS1A hexamer based on the experiment in which a sulfate ion was co-crystallized in the pore of the CsoS1A hexamer.[17] The sulfate ion was chosen because it is negatively charged and the CsoS1A hexamer has a slight positive charge across the pore. However, Tsai et al. were not able to obtain co-crystals with the negatively charged molecules bicarbonate and RuBP, which are both required to cross the carboxysome shell for CO_2

fixation to occur in the carboxysome.[17] The -2 charge of sulfate may allow for a stronger electrostatic interaction with the pore than the -1 charge on bicarbonate. RuBP has a -4 charge due to the phosphates but its structure is more bulky than that of the bicarbonate or sulfate ion. The CsoS1A hexamer pore is 4-5 Å in diameter, which may accommodate a small molecule such as bicarbonate, but the larger structure of RuBP may have some steric hindrance with the structure of the pore.[17] Therefore, the growth characteristics of the F40D pore mutant may be due to the change in the surface charge of the hexamer, which may be hindering the diffusion of negatively charged RubisCO metabolites across the carboxysome shell.

Polypeptide Composition of Purified Mutant Carboxysomes

Western blots were performed to test for the presence of the different polypeptides that make up the mutant carboxysomes when compared to the wild type carboxysomes. According to the Western blots, the abundance of each of the polypeptides that make up the mutant carboxysomes were comparable to wild type carboxysomes; however, the CsoS1D polypeptides were more abundant in the mutant carboxysomes when compared to wild type carboxysomes. The amount of CsoS1D polypeptide in carboxysome of the F40D mutant was less when compared to the amount of CsoS1D polypeptide in the carboxysome of G42L pore mutant. The additional CsoS1D polypeptide could be seen only after blotting with antibodies against CsoS1D and not in the SDS-PAGE stained with Coomassie blue. Since CsoS1D is a minor shell component in the carboxysome, it is unclear what the advantages are for having increased amounts of CsoS1D. Roberts et al. created a mutant in which the *csoS1D* gene was replaced with a kanamycin cassette.[61] The CsoS1D deletion mutant grew poorly in

ambient air and grew to a comparable maximum cell density to wild type cultures when grown in air supplemented with 5% CO_2. The removal of CsoS1D from the carboxysome shell clearly affects the growth of *H. neapolitanus* in air. Although the protein is a minor shell component, CsoS1D pseudohexamers may play a role in metabolite flux due to the large 14 Å possibly gated pore that may provide a way for RubisCO metabolites to diffuse across the shell.

Structure, Size, and Stability of the Carboxysome Pore Mutants

The purified carboxysomes of the pore mutants and wild type were observed using the transmission electron microscope. The overall size and structure of the carboxysome pore mutants were similar to wild type carboxysomes. Based on RubisCO release experiments the mutant carboxysomes appeared to be stable (Figure 20). Therefore, it appears that the pore mutants were able to express and assemble carboxysomes similar to wild type. Also, the increased amount of CsoS1D polypeptide in the carboxysome of each of the pore mutants didn't appear to affect the size and structure of the carboxysome when compared to wild type carboxysome. This result coincides with the observations made by Roberts et al. in the electron microscopic study of the carboxysomes from the *H. neapolitanus* CsoS1D deletion mutant, which revealed that size and structure of the carboxysomes were not affected by the deletion of CsoS1D from the carboxysome shell.[61]

CHAPTER VI

CONCLUSIONS AND FUTURE WORK

Conclusions

The first conclusion drawn from this study was that the size of the pore may affect the growth characteristics of *H. neapolitanus* based on the high CO_2-requiring phenotype of the G42L pore mutant. Further testing is needed to determine the role of the CsoS1D pseudohexamer in RubisCO metabolite diffusion. Based on the experiments by Roberts, it is known that the carboxysome needs CsoS1D due to the HCR phenotype that resulted when the *csoS1D* gene was deleted from the genome of *H. neapolitanus*.[61] It can not be concluded that the elevated optimal density reading of the G42L pore mutant when grown in air supplemented with 5% CO_2 was due to the presence of more cells in the culture or an excess amount of insoluble sulfur in the media that could not be efficiency removed before the optical density reading was taken. Further testing will be needed to determine if the growth characteristics of G42L pore mutant were based on just the change to the pore or if there were other factors, such differences in the oxidation of sulfur, intermediate oxidation, or the upregulation of Form II RubisCO. The carboxysomes of the G42L pore mutant had a similar size, shape, and stability as the wild type carboxysomes based on the electron micrographs and the RubisCO release experiment.

Based on the difference in the growth rate between F40D pore mutant and wild type, it can be concluded that the surface potential of the pore may play a role in affecting the growth characteristics of *H. neapolitanus*. The biphasic growth rate of the F40D pore mutant may be due to the reduced energy from the sulfur oxidation pathway and reducing

agents, which will prevent the CO_2 acceptor RuBP from being regenerated in the Calvin-Benson-Bassham cycle. Reduction of RuBP will slow down carbon dioxide fixation, which will hinder the growth of the cells. The elevated levels of CsoS1D and the change in the surface charge of the hexamer pore in the carboxysomes of the F40D pore mutant didn't appear to affect the structure, size, and stability of carboxysomes based on the electron micrographs and RubisCO release experiment.

Future Work

Currently, it has not been determined if the hexamers are homohexamers or heterohexamers. The crystal structure of the CsoS1A hexamer was obtained by using recombinant CsoS1A (rCsoS1A).[17] To test if heterohexamers can form *in vitro*, all three recombinant CsoS1 paralogs can be mixed together and co-crystallized. It also needs to be determined if the mutated CsoS1A protein is being incorporated into the carboxysome. Since CsoS1C and CsoS1A are 98% identical, the primary structures of these proteins differ by only two of the 98 amino acids. CsoS1C may be incorporated into the carboxysome instead of CsoS1A, or they are incorporated at a different ratio than observed in wild type carboxysomes. To determine if the altered CsoS1A polypeptide is being incorporated into the carboxysome shell, tagging with a His_6 will increase the mass of CsoS1A. The change in mass of the CsoS1A polypeptide can be visualized using SDS-PAGE. Additional *H. neapolitanus* CsoS1 pore mutants may need to be created in which the pore motif of CsoS1C and/or CsoS1B are altered.

The investigation involving the elucidation of expected interacting protein partners that form the functional carboxysome will need to be continued by transforming *H. neapolitanus* with the plasmid constructs that encode each His_6-tagged CsoS1 paralog.

The next step will involve purifying the carboxysomes from each of the His_6-tagged CsoS1 *H. neapolitanus* mutants using the method outlined by Cannon and Shively.[9] Next the His_6-tagged CsoS1 carboxysomes will be affinity purified using a Ni^{2+}-NTA column. Due to the presence of the His_6-tagged CsoS1 in the carboxysome shell, it is predicted that the carboxysome will remain bound to the Ni^{2+}-NTA only if the His_6-tag is oriented outside the carboxysome. If the carboxysome remains on the column, then the sidedness of the hexamers in the carboxysome can be determined. If the carboxysomes remain on the column, then they will be slightly denatured using 1 M urea that should not disrupt the interacting protein partners. This experiment should allow for the His_6-tagged proteins and any interacting proteins to remain on the column, and the interacting protein partners with His_6-tagged CsoS1 paralogs can be separated from the unbound proteins. The elution fractions will be analyzed using SDS-PAGE and Western blots that will identify the proteins interacting with the His_6-tagged CsoS1 paralogs.

APPENDIX A

OLIGONUCLEOTIDES FOR THE GENERATION OF CSOS1A PORE CONSTRUCTS

Mutant	Primer Name	Sequence	Description
G42L	*csoS1 PmI*I Fwd	5'-ACACGTGG CTTAGTTC CTGC-3'	Forward primer which was homologous to the 5' region of *csoS1A* gene and included the *PmI*I enzyme restriction site
	csoS1 G42L Rev	5'-GTAACCGC CAAGAACA AATT-3	Reverse primer which was homologous to a region of the *csoS1A* gene and contained the desired mutation
	csoS1 G42L Fwd	5'-AATTTGTT CTTGGCGG TTAC-3'	Forward primer which was homologous to a region of the *csoS1A* gene and contained the desired mutation
	csoS1 *Bsu*36I Rev	5'-CGCCTTAG GCAGAATG TTTT-3'	Reverse primer which was homologous to the 3' region of the *csoS1A* gene and included the *Bsu*36I enzyme restriction site
F40D	csoS1 *PmI*I Fwd	5'-ACACGTGG CTTAGTTC CTGC-3'	Forward primer which was homologous to the 5' region of *csoS1A* gene and included the *PmI*I enzyme restriction site
	csoS1 F40D Rev	5'-CCACCAAC ATCTTGAC GACC-3'	Reverse primer which was homologous to a region of the *csoS1A* gene and contained the desired mutation
	csoS1 F40D Fwd	5'-GGTCGTCA AGATGTTG GTGG-3'	Forward primer which was homologous to a region of the *csoS1A* gene and contained the desired mutation
	csoS1 Bsu36I Rev	5'-CGCCTTAG GCAGAATG TTTT-3'	Reverse primer which was homologous to the 3' region of the *csoS1A* gene and included the *Bsu*36I enzyme restriction site

APPENDIX B

OLIGONUCLEOTIDES FOR THE GENERNATION OF CSOS1A HIS_6-TAGGED CONSTRUCTS

Mutant	Primer Name	Sequence	Description
C-Terminally His_6-tagged CsoS1A	1A-Kan Primers	5'-CGTGTCCACTCAGAAGTAGAAAACATTCTGCCTAAGGCGCCAGCCCACCATCACCATCACCATTAACCGGAATTGCCAGCTGGG-3'	Forward primer which annealed to the 5' region of the *Kan* cassette and included a region that was homologous to the 3' region of *csoS1A* and included six His codons
	1A-Kmr	5'-GGTTTCGGCGACGGGTGTCGCCGAAGTGAGCCGTCTTAGGAAATATCTGACTCAGAAGAACTCGTCAAGAAGGCG-3	Reverse primer which annealed to the 3' region of the *Kan* cassette and included a region that was homologous to the intergenic region between *csoS1A* and *csoS1B*
C-Terminally His_6-tagged CsoS1C	*BamH*I-1Cdwn-His-KmP Fwd	5'-GGATCCTCCGAAGTCGAAAAGATCCTGCCGAAAGCCCCTGAAGCTCACCATCACCATCACCATTAACCGGAATTGCCAGCTGGG-3'	Forward primer which annealed to the 5' region of the *Kan* cassette and included a region that was homologous to the 3' region of *csoS1C* and included six His codons and a *BamH*I enzyme restriction site
	*Xho*I-1Aupstm-KmRev Comp	5'-CTCGAGAACCGGAACAAGCCTGCCCCGGTTCGTCTTTCCCAATCCTCAGAAGAACTCGTCAAGAAGGCGATAGAAGGCGATGCGC-3'	Reverse primer which annealed to the 3' region of the *Kan* cassette and included a region homologous to the intergenic region between *csoS1C* and *csoS1A* and a *Xho*I enzyme restriction site
N-Terminally His_6-tagged CsoS1B	5' 1B-His-Fwd	5'-CACGTGGCTTAGTTCCTGCG-3'	Forward primer which annealed to the 5' region of *csoS1A*
	5' 1B-His-Rev	5'-ATGGTGATGGTGATGGTGCATAACAGATCCTCTAAAACTAGTGTTGACCAC-3'	Reverse primer which annealed to the 5' region of *csoS1B* and included six His codons
	3' 1B-His-Fwd	5'-CACCATCACCATCACCATATGGCAACGACTCACGGTAT-3'	Forward primer which annealed to the 5' region of *csoS1B* and contained six His codons
	1Br7794	5'-TCGGGCGTCTCGGGTAGG-3'	Reverse primer which annealed downstream of *csoS1B*

REFERENCES

(1) Shively, J. M. *Annu. Rev. Microbiol.* **1974**, *28*, 167-188.

(2) Lanaras, T.; Cook, C. M.; Wood, A. P.; Kelly, D. P.; Codd, G. A. *Arch. Microbiol.* **1991**, *156*, 338-343.

(3) Holthuijzen, Y. A.; Breemen, J. F. L.; Kuenen, J. G.; Konings, W. N. *Arch. Microbiol.* **1986**, *144*, 398-404.

(4) Kaplan, A.; Helman, Y.; Tchernov, D.; Reinhold, L. *Proc. Natl. Acad. Sci. U. S. A.* **2001**, *98*, 4817-4818.

(5) Codd, G. A. *Adv. Microb. Physiol.* **1988**, *29*, 115-64.

(6) Codd, G. A.; Marsden, W. J. N. *Biol. Rev.* **1984**, *59*, 389-422.

(7) Miziorko, H. M.; Lorimer, G. H. *Annu. Rev. Biochem.* **1983**, *52*, 507-35.

(8) Holthuijzen, Y. A.; Kuenen, J. G.; Konings, W. N. *FEMS Microbiol. Lett.* **1987**, *42*, 121-124.

(9) Cannon, G. C.; Shively, J. M. *Arch. Microbiol.* **1983**, *134*, 52-59.

(10) Dou, Z.; Heinhorst, S.; Williams, E. B.; Murin, C. D.; Shively, J. M.; Cannon, G. C. *J. Biol. Chem.* **2008**, *283*, 10377-10384.

(11) Shively, J. M.; Lorbach, S. C.; Jin, S.; Baker, S. H. In *Microbial Growth on C1 Compounds*; Lidstrom, M. E., Tabita, F. R., Eds.; Kluwer: Dordrecht, The Netherlands, 1996, 56-63.

(12) Roberts, E. W.; Cai, F.; Kerfeld, C. A.; Cannon, G. C.; Heinhorst, S. *J. Bacteriol.* **2012**, *194*, 787-95.

(13) Tanaka, S.; Kerfeld, C. A.; Sawaya, M. R.; Cai, F.; Heinhorst, S.; Cannon, G. C.; Yeates, T. O. *Science* **2008**, *319*, 1083-1086.

(14) Baker, S. H.; Lorbach, S. C.; Rodriguez-Buey, M.; Williams, D. S.; Aldrich, H. C.; Shively, J. M. *Arch. Microbiol.* **1999**, *172*, 233-239.

(15) Heinhorst, S.; Cannon, G. C.; Shively, J. M. In *Complex Intracellular Structures in Prokaryotes*; Shively, J. M., Ed.; Springer: Berlin/Heidelberg, **2006**; Vol. 2, pp 141-164.

(16) So, A. K.-C.; Espie, G. S.; Williams, E. B.; Shively, J. M.; Heinhorst, S.; Cannon, G. C. *J. Bacteriol.* **2004**, *186*, 623-630.

(17) Tsai, Y.; Sawaya, M. R.; Cannon, G. C.; Cai, F.; Williams, E. B.; Heinhorst, S.; Kerfeld, C. A.; Yeates, T. O. *PLoS Biol.* **2007**, *5*, e144.

(18) Williams, E. B. Ph.D. Dissertation, The University of Southern Mississippi, Hattiesburg, MS, August 2006.

(19) Kelley, L. A.; MacCallum, R. M.; Sternberg, M. J. E. *J. Mol. Biol.* **2000**, *299*, 499-520.

(20) Vishniac, W.; Santer, M. *Bacteriol. Rev.* **1957**, *21*, 195-213.

(21) Kuenen, G.; Bos, P. In *Autotrophic Bacteria*; Schlegel, H. G., Bowien, B., Eds.; Science Tech: Madison, WI, **1989**, p 53-80.

(22) Pronk, J. T.; Meulenburg, R.; Hazeu, W.; Bos, P.; Kuenen, J. G. *FEMS Microbiol. Rev.* **1990**, *75*, 293-306.

(23) Bassham, J. A.; Benson, A. A.; Calvin, M. *J. Biol. Chem.* **1950**, *185*, 781-7.

(24) Campbell, N.; Reece, J. *Campbell Biology*, Ed. 7th; Pearson Education, Inc.: San Francisco, CA, 2005, pp 185.

(25) Tabita, F. R.; Hanson, T. E.; Li, H.; Satagopan, S.; Singh, J.; Chan, S. *Microbiol. Mol. Biol. Rev.* **2007**, *71*, 576-599.

(26) Hartman, F. C.; Harpel, M. R. *Annu. Rev. Biochem.* **1994**, *63*, 197-234.

(27) Harpel, M. R.; Lee, E. H.; Hartman, F. C. *Anal. Biochem.* **1993**, *209*, 367-374.

(28) Tabita, F. R.; Satagopan, S.; Hanson, T. E.; Kreel, N. E.; Scott, S. S. *J. Exp. Bot.* **2008**, *59*, 1515-1524.

(29) Jordan, D. B.; Ogren, W. L. *Nature* **1981**, *291*, 513-515.

(30) Andersson, I.; Backlund, A. *Plant Physiol. Biochem.* **2008**, *46*, 275-291.

(31) Toyoda, K.; Yoshizawa, Y.; Arai, H.; Ishii, M.; Igarashi, Y. *Microbiology* **2005**, *151*, 3615-25.

(32) Shively, J. M.; English, R. S. *Can. J. Bot.* **1991**, *69*, 957-962.

(33) Badger, M. R.; Price, G. D. *Physiol. Plant.* **1992**, *90*, 529-536.

(34) Dobrinski, K. P.; Longo, D. L.; Scott, K. M. *J. Bacteriol.* **2005**, *187*, 5761-5766.

(35) Badger, M. R.; Price, G. D. *Plant Physiol.* **1989**, *89*, 51-60.

(36) Price, G. D.; Badger, M. R.; Woodger, F. J.; Long, B. M. *J. Exp. Bot.* **2008**, *59*, 1441-1461.

(37) Badger, M. R.; Price, G. D. *J. Exp. Bot.* **2003**, *54*, 609-622.

(38) Cannon, G. C.; Baker, S. H.; Soyer, F.; Johnson, D. R.; Bradburne, C. E.; Mehlman, J. L.; Davies, P. S.; Jiang, Q. L.; Heinhorst, S.; Shively, J. M. *Curr. Microbiol.* **2003**, *46*, 115-119.

(39) Shively, J. M.; Bock, E.; Westphal, K.; Cannon, G. C. *J. Bacteriol.* **1977**, *132*, 673-675.

(40) Ebert, A. Ph.D. Dissertation, University of Hamburg, Hamburg, Germany 1982.

(41) Badger, M. R.; Hanson, D.; Price, G. D. *Funct. Plant Biol.* **2002**, *29*, 161-173.

(42) Baker, S. H.; Williams, D. S.; Aldrich, H. C.; Gambrell, A. C.; Shively, J. M. *Arch. Microbiol.* **2000**, *173*, 278-283.

(43) Dou, Z. Ph.D. Dissertation, The University of Southern Mississippi, Hattiesburg, MS, May 2009.

(44) Klein, M. G.; Zwart, P.; Bagby, S. C.; Cai, F.; Chisholm, S. W.; Heinhorst, S.; Cannon, G. C.; Kerfeld, C. A. *J. Mol. Biol.* **2009**, *392*, 319-333.

(45) Cai, F. Ph.D. Dissertation, The University of Southern Mississippi, Hattiesburg, MS, August 2009.

(46) Badger, M. R. *Photosynth. Res.* **2003**, *77*, 83-94.

(47) Yeates, T. O.; Kerfeld, C. A.; Heinhorst, S.; Cannon, G. C.; Shively, J. M. *Nat. Rev. Micro.* **2008**, *6*, 681-691.

(48) Kinney, J. N.; Axen, S. D.; Kerfeld, C. A. *Photosynth. Res.* **2011**, *109*, 21-32.

(49) Shively, J. M.; Ball, F. L.; Kline, B. W. *J. Bacteriol.* **1973**, *116*, 1405-1411.

(50) Holthuijzen, Y. A.; Breemen, J. F. L.; Konings, W. N.; Bruggen, E. F. J. *Arch. Microbiol.* **1986**, *144*, 258-262.

(51) Price, G. D.; Badger, M. R. *Can. J. Bot.* **1991**, *69*, 963-973.

(52) Orus, M. I.; Rodriguez, M. L.; Martinez, F.; Marco, E. *Plant Physiol.* **1995**, *107*, 1159-1166.

(53) Menon, B. B.; Dou, Z.; Heinhorst, S.; Shively, J. M.; Cannon, G. C. *PLoS ONE* **2008**, *3*, e3570.

(54) Baker, S. H.; Jin, S.; Aldrich, H. C.; Howard, G. T.; Shively, J. M. *J. Bacteriol.* **1998**, *180*, 4133-4139.

(55) English, R. S.; Lorbach, S. C.; Huffman, K. M.; Shively, J. M. *Appl. Environ. Microbiol.* **1995**, *33*, 1-6.

(56) Cai, F.; Menon, B. B.; Cannon, G. C.; Curry, K. J.; Shively, J. M.; Heinhorst, S. *PLoS ONE* **2009**, *4*, e7521.

(57) Yu, D.; Ellis, H. M.; Lee, E.-C.; Jenkins, N. A.; Copeland, N. G.; Court, D. L. *Proc. Natl. Acad. Sci. U.S.A.* **2000**, *97*, 5978-5983.

(58) English, R. S.; Jin, S.; Shively, J. M. *Appl. Environ. Microbiol.* **1995**, *61*, 3256-3260.

(59) Starkey, R. L. *J. Bacteriol.* **1925**, *10*, 135-63.

(60) Yoshizawa, Y.; Toyoda, K.; Arai, H.; Ishii, M.; Igarashi, Y. *J. Bacteriol.* **2004**, *186*, 5685-5691.

(61) Roberts, E.; Cai, F.; Hirst, W.; Veldkamp, A. A.; Crump, C. D.; Kerfeld, C. A.; Cannon, G. C.; Heinhorst, S. The Novel Shell CsoS1D Limits Flux of the RubisCO Product, 3-PGA, Out of the Carboxysome, unpublished manuscript.